In: Recent Studies in Materials Science ISBN 978-1-53615-270-8
Editor Patrick R. Lind

Chapter 3

OSCILLATORY AND TURBULENT FLOWS OF LIQUID METALS IN DIFFERENTIALLY HEATED SYSTEMS WITH HORIZONTAL AND NON-HORIZONTAL WALLS

Marcello Lappa and Hermes Ferialdi*
Department of Mechanical and Aerospace Engineering,
University of Strathclyde, Glasgow, UK

ABSTRACT

Non isothermal flows of liquid metals induced by buoyancy are central to many advanced technological applications in materials science, often at the cutting-edge of modern engineering. They have indeed a significant impact on the production of many materials obtained via the solidification of a melt. The quality and mechanical or electrical properties of the resulting solids and crystals are adversely affected by thermogravitational convection as it can induce defects in their atomic or

* Email: Marcello.lappa@strath.ac.uk.

molecular structure (this is the case, e.g., of typical crystal-growth techniques such as the horizontal Bridgman (HB), the Floating zone (FZ) or the Czochralski (CZ) methods). The present chapter aims to present a focused review of landmark (past) and very recent contributions on the nature, structure and hierarchy of instabilities of this type of convection. In particular, starting from simple situations corresponding to steady and laminar flows and moving towards fully developed turbulence, we present the typical hydrodynamic and hydrothermal disturbances emerging in differentially heated liquid metals and clarify the relationship among their properties and general influential factors such as: the degree of confinement (aspect ratio), morphology (wall orientation in space) and spatial degrees of freedom (number of active dimensions) of the domain hosting the melt. Manifestations of these modes of convection (including, but not limited to, transverse waves travelling in the downstream or in the upstream direction, standing waves, modulated pulso-traveling disturbances, longitudinal waves and multi-wave patterns) are discussed in detail. More complex situations are placed in the context of existing theories on turbulence in fluids and treated using concepts, methods and tools typical of the chaotic systems analysis.

1. INTRODUCTION

Flows of liquid metals are pervasive in a number of technological applications in different fields. This is indeed the case of many manufacturing activities where the considered product passes through a liquid state before being solid. Relevant examples can obviously be found in the foundry and metallurgical sectors and in the cognate field of crystal growth from the melt.

Engineers have often to deal with such flows, given the impact they have on the considered processing techniques and the quality of resulting materials. This is especially true, when the considered materials are used for advanced applications where the perfection of the crystalline structure is a necessary pre-requisite (e.g., semiconductors and superconductors). Indeed, the properties of the flow, i.e., its structure in space and evolution in time, can deeply influence the solidification process (typically convective disturbances of various types can produce defects in the material chemical structure at the micro or macro scale in the form of

"striations" or "segregations", respectively; Dupret and Van der Bogaert, 1994; Monberg, 1994).

In most cases, such flows are produced by buoyancy effects, i.e., they result from the action exerted by Earth's gravitational field on the small density differences which are induced in the liquid by existing temperature differences or non-uniformities. Though a vast literature has been produced to describe this kind of motion and related instabilities, liquid metals have their own characteristic modes of convection, which differentiate them from known behaviors in other (common) liquids such as water or other transparent melts (such as molten oxide materials or plastics, Lappa, 2019, Lappa and Ferialdi, 2018).

In such a context, this chapter will give the reader the opportunity to identify and explore a number of advanced topics in heat transfer and fluid flow, which relate to metal substances in the molten state. More specifically, starting from the review of existing literature and related historical background, in line with the general spirit of this book, we will consider the limitations of current knowledge and the new results that engineers are producing towards the end to fill existing gaps. Where appropriate, we will use computational fluid dynamics techniques and related results to support the discussions and provide evidence/exemplars for the described dynamics.

For the convenience of the reader, using a deductive approach, first the simplest theoretically possible situation will be considered, that is, thermogravitational flow developing in a horizontally unbounded layer of infinite extent. Then, more complex and realistic circumstances will be addressed in terms of shape of the containers and spatial degrees of freedom.

1.1. The Hadley Flow: Historical Background

Given the complex (often counter-intuitive) behavior displayed by these fluid-dynamic processes and their evolution in time, over the years the investigators have conceived simplified geometrical configurations to

study the response of thermogravitational flow to changes in the applied temperature gradients.

Historically, the first model elaborated in such a process of abstraction is represented by the so-called *Hadley flow* (Hadley, 1735), namely, the horizontally elongated unicellular circulation induced by a horizontal temperature gradient in a fluid domain of finite extent (heated at one side and cooled at the other side). Over subsequent years, however, other researchers further simplified this configuration by concentrating on the central portion of such flow assumed not to be influenced by edge effects. This has naturally led to the introduction of the so-called 'infinite layer model', extensively employed for the identification of the typical modes of convection of the Hadley flow and related instabilities (Hart, 1972 and 1983; Gill, 1974; Laure and Roux, 1989; Kuo and Korpela, 1988; Gershuni et al., 1992).

Assuming an unbounded system and the related flow to be 'parallel' (i.e., flow with a single velocity component in the same direction of the applied temperature gradient), indeed, implies an important intrinsic advantage. It has proved very effective and convenient for the application of typical linear stability analysis (LSA) protocols, especially in the era when efficient computers for the numerical solution of the overarching non-linear equations (the so-called Navier-Stokes equations coupled with the energy balance equation) were not available yet.

LSA is the art of deducing fundamental information on the behavior (in terms of possible evolution) of certain solutions of these equations working on alternative versions of them derived through linearization. Though with some limitation (LSA cannot yield quantitative data on the effective intensity of the emerging flow), this approach has enjoyed a widespread use in the literature for its known ability to provide meaningful information on the fundamental modes of instability of several flows for which the 'basic' states were known.

For the Hadley flow, in particular, these modes can be categorized as 'transverse' and 'longitudinal'. This denomination originates from the orientation in space of the emerging rolls that, by adding new velocity

components to the original basic velocity profile, break the uniformity of the initial state (the parallel flow).

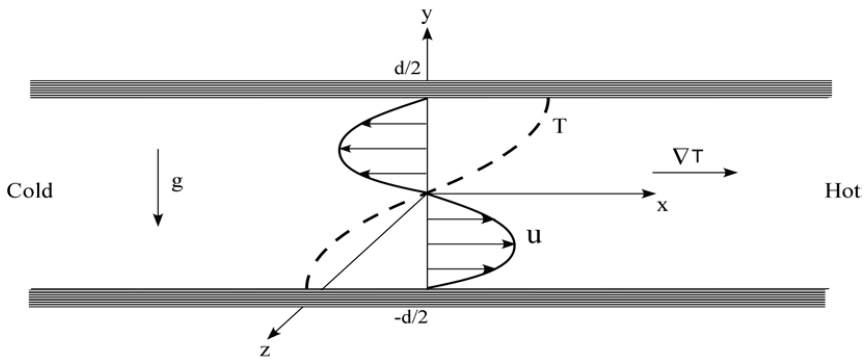

Figure 1. Basic-state velocity profile and related temperature distribution for thermal convection in an infinitely extended horizontal liquid layer delimited vertically by rigid adiabatic (thermally insulated) walls.

In other words, this means that starting from initial conditions such as those illustrated in Figure 1, the Hadley convection in an infinite layer can develop rolls with either of the orientations shown in Figure 2.

These modes differ in the spatial structure of the rolls and the angle they form with the imposed temperature gradient (transverse and longitudinal rolls having their axes perpendicular and parallel to the gradient, respectively). A significant distinguishing mark, however, also relates to the 'mechanisms' able to produce these flow features, i.e., the genesis of these convective disturbances.

The instability leading to transverse rolls is generally considered as a 'hydrodynamic' effect because it is driven by the mean shear stress that arises as a consequence of the different direction of the currents going from the hot to the cold side in proximity to the top of the layer and vice versa near the bottom. This is the reason why it is often referred to as "shear instability" and the related features as hydrodynamic disturbances. As a result, the initial 'unicellular' Hadley flow is replaced by a multicellular convective structure consisting of a chain of rolls extended along the frontier of the two opposing (primary and return) horizontal currents

(Figure 2a). These rolls are stationary and become oscillatory when a second threshold in terms of applied temperature gradient is exceeded (Gelfgat et al., 1999).

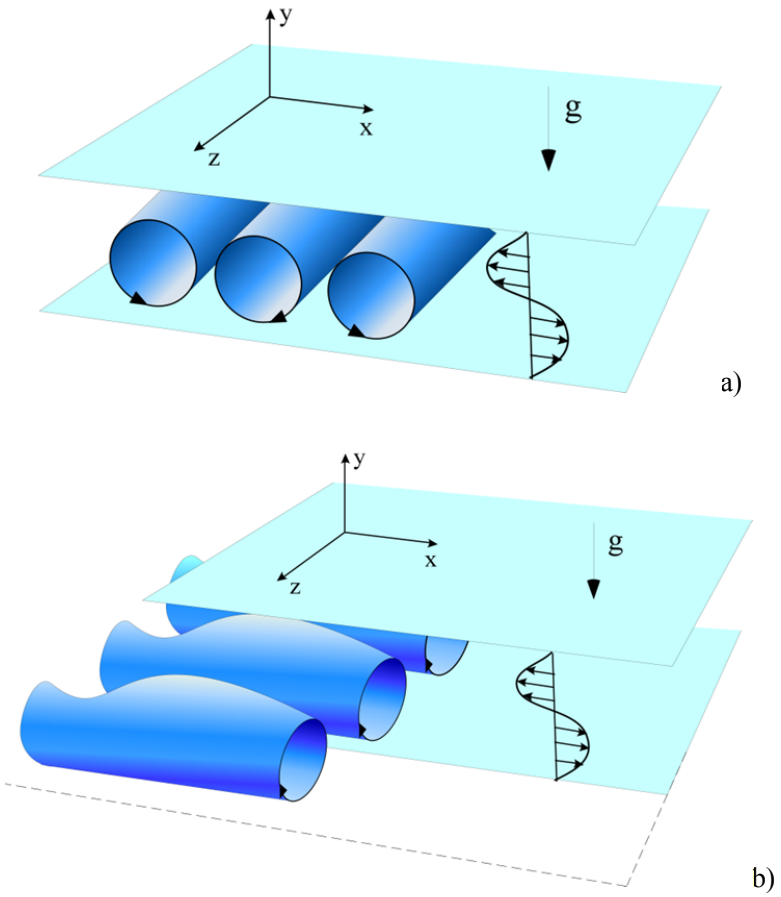

Figure 2. Sketch of convection with: a) a set of (transverse) rolls perpendicular to the imposed temperature gradient; b) a set of (longitudinal) rolls parallel to the imposed temperature gradient.

The physical process leading to the longitudinal instability is slightly more complex as it involves some interplay between the mean shear stress and the buoyancy force (a dynamical balance that makes thermal effects *directly relevant to the instability mechanism*, from which the

denomination of "hydrothermal disturbances"). Hereafter, hydrodynamic and hydrothermal modes will therefore be used as synonyms for the transverse and longitudinal instabilities, respectively (the latter is also known as OLR, i.e., Oscillatory Longitudinal Roll mode of convection). Perhaps, it is also worth mentioning that in the literature the hydrothermal modes have also been called 'helical waves' given their nature of essentially travelling disturbances. This alternate nomenclature also directly follows from the superposition of the basic parallel Hadley flow and the longitudinal rolls, which force fluid particles to move along helical paths (Figure 2b).

The main results provided by the LSA for the parallel Hadley flow in an unbounded layer are summarized in Figure 3. This figure shows that different modes can exist in specific ranges of the so-called Prandtl number. This non-dimensional number, defined as the ratio of the melt kinematic viscosity and its thermal diffusivity ($Pr = \nu/\alpha$), takes a different value according to the substance considered. For liquid metals and semiconductor melts, in general, it is much smaller than 1.

In Figure 3 it can be seen that the conditions required for the onset of these convective disturbances are given in terms of critical *Grashof Number*, $Gr = g\beta_T\gamma d^4/\nu^2$, where γ is the rate of temperature increase along the horizontal direction (assumed to be constant by linear stability analyses), d is the thickness of the considered layer and β_T is the so-called thermal expansion coefficient. Sometimes, the instability thresholds are also reported in terms of the so-called Rayleigh number, related to the Grashof and Prandtl numbers by the simple relationship $Ra = GrPr$.

As evident in this figure, the emerging disturbances are essentially two-dimensional (2D) for relatively small values of the Prandtl number (transverse rolls), while they are taken over by 3D effects (OLR rolls) as Pr approaches 0.1. This observation becomes even more interesting if it is considered in combination with *existing theorems* on the stability of fluids.

The presence of inflection points in the velocity profile for purely parallel flow (see Figure 1), indeed, is known to play an important role if it is considered together with the so-called Rayleigh's theorem. According to this theorem: "*In an inviscid shear flow a necessary condition for*

instability is that there must be a point of inflection in the velocity profile u = u(y), i.e., a point where $d^2u/dy^2 = 0$*"*. Many authors (Tollmien, 1936; Lin, 1944; Rosenbluth and Simon, 1964; Drazin and Howard, 1966) proved that this necessary condition can also be 'sufficient' in many circumstances. Squire (1933) demonstrated that the related disturbances are purely two-dimensional.

Such arguments would indeed confirm the results of the LSA about the 2D nature of the disturbances in the limit as Pr tends to zero (inviscid flow).

The Squire's theorem, however, is no longer applicable when the Prandtl number is not exactly zero (in such a case momentum and energy cannot be uncoupled, which also invalidates the outcomes of the Rayleigh theorem). This indirectly confirms the observed 3D nature of the modes emerging for increasing values of Pr.

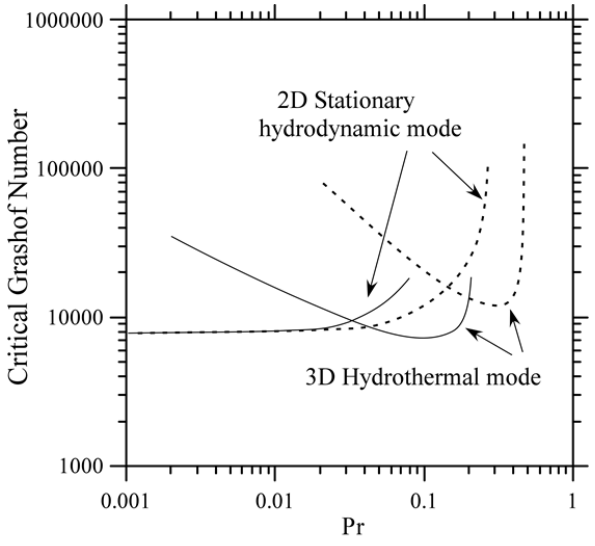

Figure 3. Stability boundaries for thermogravitational convection in an infinite layer delimited by horizontal solid walls with different thermal conditions: adiabatic (solid line) and conducting (dashed line) boundaries (Grashof number defined as $Gr = g\beta_T\gamma d^4/\nu^2$ where γ is the uniform rate of temperature increase along the x axis; courtesy of P. Laure).

Interestingly, Figure 3 also shows that the threshold values for hydrodynamic or hydrothermal disturbances depend on the nature of the thermal boundary conditions assumed for the top and bottom walls. For the case with adiabatic walls, indeed, the 3D oscillatory mode (OLR) and the 2D stationary (hydrodynamic) branches intersect at Pr = 0.034, while the intersection point is located at Pr = 0.114 when conducting walls are considered (walls with a linear profile of temperature).

Both the 2D branches (in the adiabatic and conducting cases) asymptotically tend to a unique limit (Gr = 7942) as Pr goes to zero, which provides further evidence about the origin of these disturbances, which take their energy from inertial forces of the basic flow and can therefore survive when the velocity and the thermal fields are no longer coupled (Pr = 0).

On increasing Pr from zero, the critical Grashof grows smoothly and this must be ascribed to the increasing effect of the thermal field (which, however, as explained before, plays no direct role in the hydrodynamic instability mechanism). The tide of the hydrodynamic instability branch finally becomes very steep when the Prandtl number approaches a certain value (Pr_L). This indicates that the hydrodynamic mode is no longer allowed beyond this point. This limiting value (Pr_L = 0.1 according to Kuo and Korpela, 1988 for the adiabatic case), shifts to Pr_L = 0.2 for the conducting case.

Vice versa, when the OLR branches are considered, the critical Grashof number rapidly increases when Pr tends to zero, confirming the essentially thermal nature of these modes of convection (suppressed in the limit as Pr $\rightarrow$ 0). Also for these disturbances, however, there exists a cut-off value of Pr where the curves are constrained by vertical asymptotes (located at Pr_{L2} = 0.2 for the adiabatic case, Pr_{L2} = 0.45 for the conducting case, respectively).

At this stage (for the sake of completeness), we should recall that the description of the case with conducting walls, however, would also require consideration of a third mode of convection, not reported in Figure 3. This type of convection, generally known as “Rayleigh mode” is excited by the presence of regions of unstable thermal stratification induced by the basic

flow in proximity to the top and bottom wall (Gershuni et al., 1992). The related disturbances generally emerge in the form of stationary rolls with their axes parallel to the imposed temperature gradient (which explains why they are also known as SLR, i.e., Steady Longitudinal Rolls). The region of existence of these disturbances largely extends beyond the aforementioned asymptotes located at Pr_{L2} (Gershuni et al., 1992); this implies they can manifest in a variety of liquids, not necessarily liquid metals. Obviously, these states completely disappear when the horizontal walls are adiabatic (as in this case the aforementioned regions with unstable thermal stratification do not form).

1.2. Inclined Systems

For fluids with Pr < 1, the set of possible modes of convection can significantly be expanded with respect to those described in the preceding section if the considered layer *is inclined instead of being perfectly horizontal* (see Figure 4). The inclination indeed leads to the presence of a destabilizing vertical component of the imposed temperature gradient, which can induce other types of convective disturbances in liquid metals regardless of whether the top and bottom boundaries of the layer are insulated (adiabatic) or conducting.

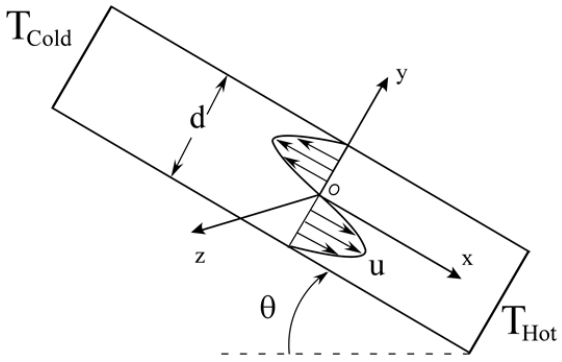

Figure 4. Sketch of differentially heated inclined rectangular box.

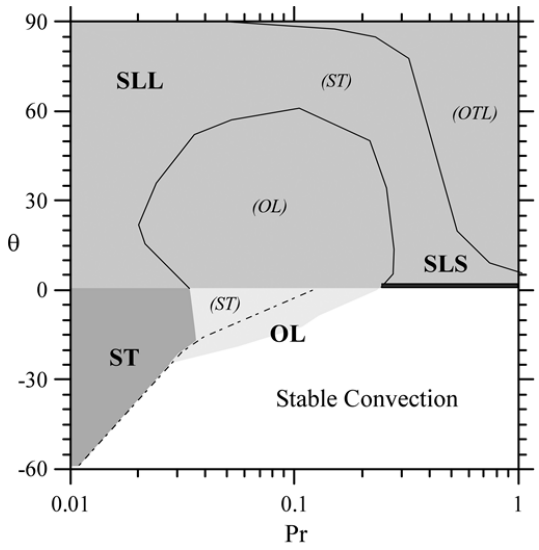

Figure 5. Instability modes in an (infinite) inclined layer with insulated walls as a function of the inclination angle and the Prandtl number (data directly provided by R. Delgado-Buscalioni). The instability with the lowest critical Rayleigh number is indicated with bold letters and that with the second lowest critical Ra is labeled in italics and between parentheses. Legend: ST (stationary transversal), OL (oscillatory longitudinal), SLL (stationary longitudinal long-wavelength), OTL (oscillatory transversal long-wavelength), SLS (stationary longitudinal short-wavelength).

The new types of instabilities in the space (θ, Pr), made possible by inclining a differentially heated cavity even if its longest walls are thermally insulated, are shown in Figure 5 and summarized in Table 1 (where some general trends have been reported for each type of instability in terms of critical Rayleigh number, defined as $Ra = g\beta_T\gamma d^4/\nu\alpha$, and wavenumber).

This problem has extensively been investigated (through LSA) by Delgado-Buscalioni and coworkers. According to their studies, the "Stationary Longitudinal long-wavelength instability" (SLL), which can appear for any $\theta < 90°$, should essentially be regarded as a 'Rayleigh mode' such as those discussed before for the horizontal layer with conducting walls. This instability is possible even if the top and bottom walls are adiabatic because by inclining the system, *the hot side can induce a heating-from-below effect*.

Table 1. Trends for the critical parameters of typical modes of instability in inclined configurations (Rayleigh number defined as $Ra = g\beta_T\gamma d^4/\nu\alpha$ where γ is the rate of temperature increase along the x axis; the configuration is assumed to have the longest walls insulated; the constants R_0, c_1, c_2 and c_3 are given in Delgado-Buscalioni, 2001)

Type of instability	Critical Ra	Critical wavenumber
ST	$\mathrm{Pr} << 1, Ra \propto \frac{\mathrm{Pr}}{\cos\theta}$ $\mathrm{Pr} \cong 1$ ($\theta < 90°$), $Ra \cong \frac{R_0}{\sin\theta}$	$q_x = 1.35$ $q_x = 1.6$
OTL	$Ra \cong \frac{R_0}{\sin\theta}$	$q_x \cong 0.3$
SLL	$Ra \cong \frac{Ra_{cr(\theta=0)}}{\sin\theta}$	$q_z = 0$
SLS	$Ra \propto \frac{\mathrm{Pr}^{1/2}}{(c_1 - \mathrm{Pr})^2}$	$q_z \cong 2.9$
OL	$Ra \propto \frac{\mathrm{Pr}^{1/2}}{(c_2 - \mathrm{Pr})^{1/2}}$	$q_z \propto \frac{(c_3 - \mathrm{Pr})^{2/5}}{\mathrm{Pr}^{-1/2}}$

The "Oscillatory Transversal long-wavelength instability" (OTL) is another instability enabled by the inclination. It is characterized by a long wavelength (typically 9 times the height d) and can emerge only if $0° < \theta < 90°$.

The other well-known classical instabilities induced by hydrodynamic or hydrothermal (OLR) disturbances for the horizontal configuration ($\theta = 90°$, see Figure 3) are also affected by the inclination. In particular, any tilt with $\theta < 90°$ tends to expand the range of existence of the stationary transverse rolls (the 2D hydrodynamic instability, which for $\theta = 90°$, as explained before, is generally observed for fluids with $\mathrm{Pr} < 0.034$ and is suppressed for $\mathrm{Pr} > \mathrm{Pr_L} \cong 0.1$). The inclination also affects the range of existence of the oscillatory longitudinal instability (OLR) (the cutoff value of Pr at which this instability is damped decreases with the inclination

angle; for example, for $\theta = 90°$ and 80° OLR perturbations are damped for $\mathrm{Pr} \geq 0.21$ and $\mathrm{Pr} \geq 0.26$, respectively).

1.3. The Non-Linear Regime: The Numerical Solution of the Navier-Stokes Equations

There is no doubt that the results provided by LSA for the horizontal or inclined infinite layer have become over the years a useful source of information for investigators interested in the fundamental gravitational modes of convection emerging in differentially heated liquid metals, and have opened new paths to a much better understanding of these fluid systems.

Unfortunately, however, the LSA is not in a condition to shed light on the behaviour of these system when they enter the non-linear regime (namely when the disturbances saturate their amplitude) as it can only provide meaningful information on the *spatial structure* of the disturbances (i.e., wavelength and wavenumber) and their *stationary or oscillatory nature*. As outlined in Sect. 1.1, estimates relating to the effective amplitude of the disturbances are out of reach because of the linearised form of the equations on which LSA relies (which prevents any information about the non-linear regime to be predicted).

This explains why, most of available results for the non-linear regime have been obtained resorting to other numerical approaches, typically based on the direct numerical solution of the Navier-Stokes equations. These equations in non-dimensional form can be cast in compact form as :

$$\underline{\nabla} \cdot \underline{V} = 0 \tag{1}$$

$$\frac{\partial \underline{V}}{\partial t} = -\underline{\nabla} p - \underline{\nabla} \cdot \left[\underline{V}\underline{V}\right] + \mathrm{Pr}\, \nabla^2 \underline{V} - \mathrm{Pr}\, Ra\ T\ \underline{i}_g \tag{2}$$

$$\frac{\partial T}{\partial t} + \underline{\nabla} \cdot \left[\underline{V} T\right] = \nabla^2 T \tag{3}$$

Where velocity and temperature have been referred to the scales α/d and ΔT, respectively and all distances have been scaled on d; accordingly, $\underline{V}$, T and p are the nondimensional velocity, temperature and pressure, respectively, $\underline{i}_g$ is the unit vector along the direction of gravity. Moreover, the Boussinesq approximation has been used for the buoyancy production term in the momentum equation.

For problem closure, the equations have to be complemented with relevant thermal and kinematic boundary conditions (BCs). While from a kinematic point of view, in general, these BCs simply reduce to setting $\underline{V} = 0$ on solid boundaries (the so-called no-slip property of walls), a wider set of variants is allowed for the temperature. If the considered wall is assumed to be isothermal, then a fixed constant temperature must be set along its entire extension; if it is thermally insulated, i.e., adiabatic, then the aforementioned Dirichlet condition corresponding to a fixed value of T must be turned into a Neumann condition on the value taken by the derivative of temperature with respect to a direction perpendicular to the boundary (this derivative must reduce to zero). If the wall behaves as a conducting surface, then a fixed-in-time distribution of temperature can again be assumed (typically a linear profile with the temperature increasing along the direction of the applied temperature gradient).

From a purely mathematical standpoint, the set of overarching equations (1-3) and related boundary and initial conditions constitute the so-called IBVP (Initial Boundary Value) problem, which elegantly encapsulates all the facets of this subject, namely, the role played by the presence of solid surfaces (walls), the specific three-dimensional shape (geometry) of the considered container and the initial conditions of the system.

Typical solution techniques of these equations, based on discretization of the considered physical domain, generally make possible (in a straightforward way in many cases) the consideration of domains of finite extent.

Apart from the general interest from the point of view of applied mathematics, which attaches to such a numerical problem, the IBVP allows

consideration of wall-effects and geometrical constraints, which, in general, can be used to explain the observed discrepancies between the predictions of the LSA for the infinite layer and the effective behavior of finite-size systems. It can also be directly linked to another very interesting aspect concerning the properties of spatially confined systems, that is, the *existence of multiple solutions* (we will come back to this very interesting concept later in this chapter).

Though many different numerical approaches are possible, in the following we concentrate on the so-called category of *projection methods*. At this stage we should clearly point out, indeed, that the practical numerical implementation of the IBVP is not independent of the specific numerical procedure considered. This apparently counter-intuitive concept originates from the realization that the adoption of a specific solution technique enriches the IBVP with additional boundary conditions. These are generally known as "numerical boundary conditions" (NBC) to distinguish them from those dictated by the physics of the considered problem. In such a context, the choice of the numerical method becomes a delicate aspect as relevant information on the proper selection of relevant NBCs making the problem well posed form a mathematical point of view is known for some cases only.

This is why for problems dealing with the study of fluid-dynamic bifurcations and eventually the existence of "multiple solutions" (we will clarify the meaning of this concept later) we recommend the use of methods pertaining to the aforementioned set of projection techniques. All the numerical examples presented in this chapter have been obtained in the framework of such approach. For this class of methods the problem relating to NBCs making the problem well posed has already been investigated to a certain extent leading to widely recognized theoretical results (Gresho and Sani, 1987; Gresho, 1991). With these methods, moreover, the problem can be tackled directly in terms of 'primitive variables' (i.e., velocity and pressure).

These techniques may be regarded as a spin-off of the strategy originally conceived by Harlow and Welch (1965), Chorin (1968) and Temam (1968) on the basis of the well-known theorem of inverse calculus

(see, e.g., Ladyzhenskaya, 1969), by which any vector function can always be decomposed into a divergence-free part $\underline{V}$ and the gradient of a scalar potential -P (a curl-free part). They are based on a simple concept, that is, the momentum equation can physically retain the correct amount of vorticity relating to the considered problem even if the contribution represented by the pressure gradient is not taken into account (from a mathematical standpoint, this property stems from the irrotational nature of every vector field resulting from the gradient of a scalar quantity):

$$\underline{V}^{*} = \underline{V}^{n} + \Delta t\left[-\underline{\nabla}\cdot\left(\underline{V}\underline{V}\right) + \mathrm{Pr}\ \ \nabla^{2}\underline{V} \right]^{n} + \mathrm{Pr}\, Ra T^{n} \underline{\hat{n}} \tag{4a}$$

The integration of the truncated momentum equation obviously leads to an intermediate velocity $\underline{V}^{*}$, which has no physical meaning. It does not even satisfy the continuity equation, in other words, it is not solenoidal. In order to correct it and make the resulting field incompressible, projection methods introduce a new velocity field as a linear combination of the unphysical velocity field $\underline{V}^{*}$ and the pressure gradient previously neglected.

$$\underline{V}^{n+1} = \underline{V}^{*} - \Delta t \underline{\nabla} p^{n} \tag{4b}$$

This approach formally leads to an additional equation required to determine the pressure, which would otherwise remain unknown. This equation is formally obtained by forcing the 'corrected' velocity field to be divergence-free. This leads to a purely elliptic equation to be solved on the basis of an iterative process (see, e.g., Lappa, 1997):

$$\nabla^{2} p^{n} = \frac{1}{\Delta t}\underline{\nabla}\cdot\underline{V}^{*} \tag{4c}$$

To make the problem well-posed, the initial velocity field $\underline{V}_0 = \underline{V}(\mathrm{t} = 0)$ must correspond to a quiescent state or satisfy the condition $\underline{\nabla}\cdot\underline{V}_0 = 0$.

Obviously, the three equations given above refer to an implementation of such a method using schemes explicit in time (the superscript n there indicates the time step). However, different variants of such approach are possible according to the philosophy used to integrate the simplified momentum equation with respect to time (via explicit or implicit schemes) and the staggered or non-staggered arrangement of primitive variables on the computational grid (see, e.g., Moukalled et al., 2016). Moreover, the accuracy of such a method obviously depends on the nature and order of the schemes used to integrate effectively the above equations and the related time and space integrations steps (such aspects are not covered here not to increase excessively the length of the chapter; the interested reader being referred to the relevant literature for additional details, e.g., Lappa and Ferialdi, 2017 and 2018b).

2. SPATIALLY CONFINED SYSTEMS

2.1. Geometrical Effects and Multiplicity of Solutions

Owing to the availability of methods for the solution of the governing equations in their complete (non-linear and time-dependent) form such as those illustrated in Sect. 1.3, over the years, configurations much more realistic than the infinite layer have been considered. Related studies have led to the more or less widespread realization that the ranges of Prandtl number and Grashof (or Rayleigh) number in which the hydrodynamic or hydrothermal modes of convection can be found depend on the effective geometry of the container hosting the melt.

An archetypal numerical study along these lines is due to Afrid and Zebib (1990), who could clearly show that the effective extension of the physical domain in the spanwise direction (the direction perpendicular to the basic flow, i.e., the z axis in Figure 1) determines a significant variation in the threshold value of the Rayleigh number. The main outcomes of these numerical simulations were confirmed by effective experiments with

opaque liquid metals (see, e.g., Hung and Andereck (1988) and Pratte and Hart (1990) for Pr = 0.026).

All these studies, conducted considering classical rectangular cavities with vertical (heated or cooled) and horizontal walls, provided reasonable hints that the location of the points in the (Ra, Pr) space where the branches pertaining to the different instability mechanisms (transverse or longitudinal) intersect might not an invariant property.

In such a context, some authors expressly focused on the possible interplay of these two fundamental modes of convection. As an example, Braunsfurth and Mullin (1996) could identify experimentally four 'apparently new' modes of oscillation for liquid metals with $0.016 \leq Pr \leq 0.022$. Similarly, through parametric numerical simulations in the interval $0 \leq Pr \leq 0.027$, Wakitani (2001) found the value of the critical Rayleigh number to grow on increasing Pr and/or by reducing the extension of the cavity in the spanwise direction. Most interestingly, these variations were *not regular*, which was interpreted as evidence for the co-existence of different oscillatory modes competing at the onset. The presence of coexisting modes of convection was also reported for supercritical conditions in the 3D numerical studies of Delgado Buscalioni et al. (2001) for inclined cavities.

Leaving aside for a while these interesting results, it should be mentioned that another interesting line of inquiry has been originated by the realisation that all these influential factors [namely, the considered melt (Pr), the control parameter (Gr or Ra), the effective spatial configuration of the container (physical domain geometry), nature of boundary conditions (top and bottom walls with adiabatic or conducting conditions) and eventually the inclination of the overall system (θ)] may not be the only ones able to affect the solutions of the aforementioned well-posed (Lappa, 2002) IBVP (Initial Boundary Value).

The initial boundary conditions can also play a significant role.

This has been revealed by a set of numerical studies originally conducted under the assumption of 2D flow (Crespo del Arco et al., 1989; Pulicani et al., 1990; Okada and Ozoe, 1993ab and Gelfgat et al., 1999), where hydrodynamic disturbances (the only ones allowed in those

circumstances) were found to produce a variety of potential behaviors, including multi-roll states, the bifurcation from steady to time-periodic solutions, the emergence of hybrid modes of convection due to the co-existence and interaction of multiple states and backward transitions from multi-roll to unicellular regimes. The most interesting of such features was, perhaps, the "multiplicity" of possible solutions, that is, the existence of distinct branches of solutions *for a fixed set of parameters*.

These studies clarified that, though such branches can exist as independent sets of solutions, the flow effectively emerging in a numerical simulation (or in the physical reality) essentially *depends on the specific initial conditions considered*.

In other words, even if the fluid (Pr), the geometry (cavity aspect ratio), the boundary conditions, the applied Gr (or Ra) and possible disturbances (hydrodynamic modes only for 2D systems) are *fixed*, the emerging flow can change in morphology (number of rolls) and nature (stationary or oscillatory) depending on the initial state of the system. Using relevant language borrowed from the companion field relating to the analysis of non-linear systems, these multiple solutions can generally be considered as coexisting 'attractors' in the space of phases (that is a space having as many dimensions as the degree of freedom of the considered system). Yet using specific technical language, it is known that in a problem developing coexisting branches of solutions, the trajectory of the system in the space of phases can tend selectively to a different attractor according to the considered "basin of attraction", which, by definition, is *the set of initial conditions that leads the system trajectory to meet a specific attractor*. An example of such behavior is shown in Figure 6.

If the numerical simulation is started from thermally diffusive conditions ($\underline{V}_0 = 0$), for a relatively low Rayleigh number, i.e., $Ra = 10^3$, the flow is simply given by a 'twisted' recirculation embracing three co-rotating (anticlockwise in the figures) rolls; this kind of flow is still a solution if, starting from the conditions shown in Figure 6a ($\underline{V}_0 \neq 0$), the Rayleigh number is increased to 2000. However, if the same simulation for Ra = 2000 is repeated assuming initial diffusive conditions, a double-vortex configuration can also be obtained; these flows are both steady and

centrally symmetric (namely, the pattern does not change with respect to rotation through 180° about the center of the cavity).

This simple example illustrates why in order to identify the window in which the system is subjected to multiple coexisting attractors, a typical strategy of analysis must be based on the exploration of the system response to a variation of the initial conditions. Put in practice, in addition to 'standard' initial conditions corresponding to a quiescent state with a diffusive distribution of temperature, other possible initial conditions must be considered (typically the solutions corresponding to one branch can be used as the initial conditions for the determination of the solutions relating to another branch, see, e.g., Kengne et al. (2018), Gelfgat et al. (1999).

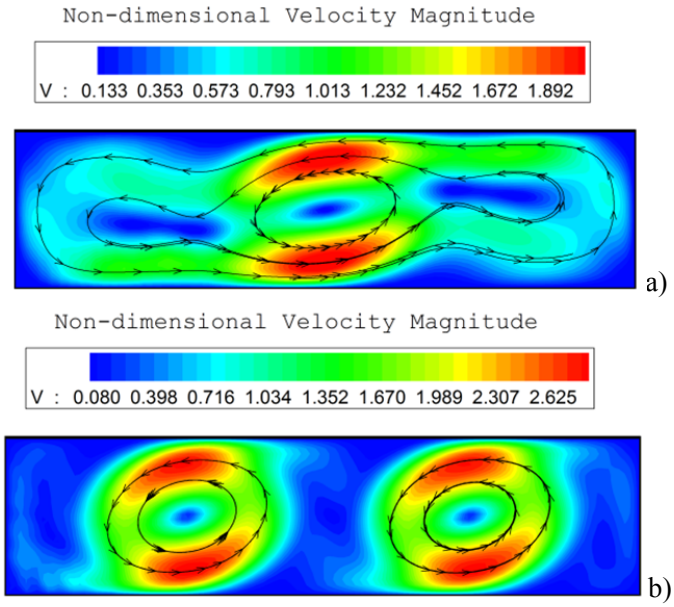

Figure 6. Multiple states of two-dimensional steady convection originating from initially thermally diffusive and quiescent conditions for a rectangular cavity with aspect ratio $A_x = L/d = 4$ (cold and hot sides on the left and on the right of each frame, respectively; upper and lower boundaries with adiabatic conditions, Rayleigh number defined as $Ra = g\beta_T \Delta T d^3/\nu\alpha$ where ΔT is the horizontal temperature difference): a) Single elongated roll for $Ra = 1x10^3$, b) two-roll state for $Ra = 2x10^3$.

2.2. Systems with Converging or Diverging Walls

This section builds on, but also seeks to extend, the valuable research that has highlighted the importance of the spatial confinement on the properties of the thermogravitational flow of liquid metals in differentially heated enclosures. In the remainder of this chapter, in particular, we concentrate on the very recent findings by Lappa and Ferialdi (2017 and 2018b) about configurations with *oppositely inclined walls* (Figure 7).

These systems may be regarded as an additional variant with respect to those traditionally considered in the past. What sets them apart is that, though the top and bottom walls are not horizontal, *no net inclination is present* (as these boundaries are one the mirror image of the other). Related studies pertain to a new line of inquiry in which, though the system is not tilted, the flow cannot be considered 'parallel'.

The geometrical configuration under examination (shown in Figure 7) is a shallow cavity symmetric with respect to the xz plane with converging or diverging walls. Its average depth is denoted by d. The lateral solid walls perpendicular to the x-axis are assumed to maintain a fixed temperature (one side cooled, the other side heated, having height d_{hot} and d_{cold}, respectively).

Three different non-dimensional (independent) parameters must therefore be introduced to characterize this problem, namely the streamwise (or transverse) aspect ratio A_x, defined as the cavity length-to-average-depth ratio $A_x = L/d$ where $d = (d_{hot} + d_{cold})/2$, the spanwise (or longitudinal) aspect ratio, $A_z = W/d$ (where W is the extension of the computational domain along z) and what we call the expansion (compression) ratio $\eta = d_{hot}/d_{cold}$ which can be > 1 (diverging geometry) or < 1 (converging geometry). In this way a more general problem is obtained in which the classical cavity with horizontal top and bottom walls considered in earlier 2D or 3D studies is just one realization (it being recovered for $\eta = 1$).

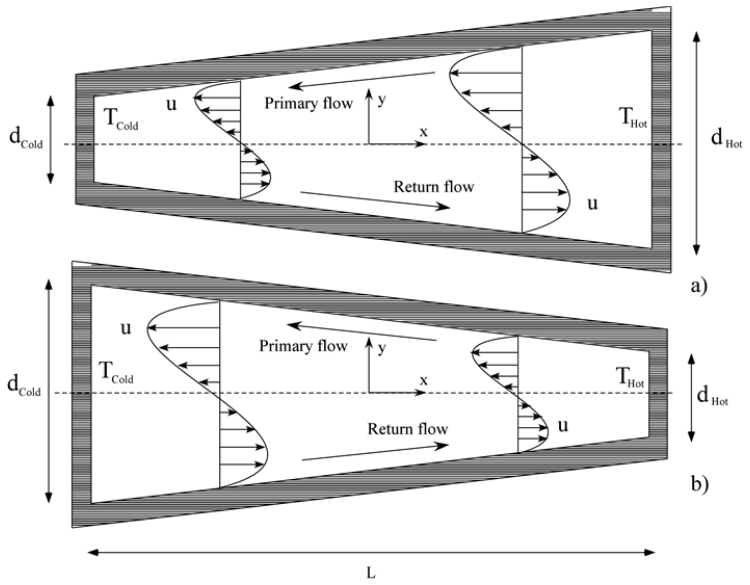

Figure 7. Sketch of enclosures with converging or diverging walls, related thermal and kinematic boundary conditions and Cartesian coordinate system: a) $\eta < 1$, b) $\eta > 1$.

In order to filter out the presence of Rayleigh modes such as those identified by Gershuni et al. (1992) for the case of conducting boundaries (which would further increase the complexity of the analysis as discussed at the end of Sect. 1.1) we assume the top and bottom walls to be adiabatic (no heat exchange). The considered system is also prevented from developing Rayleigh modes such as those reported by Delgado Buscalioni et al. (2001) for inclined cavities (see Sect. 1.2) as in the present case the heated and cooled walls remain always perfectly vertical (thereby excluding the presence of destabilizing vertical components of the temperature gradient, i.e., components potentially leading to *a heating-from-below effect*).

As sketched in Figure 7, the natural buoyancy flow emerging is such configurations for relatively small values of the Rayleigh number ($Ra = GrPr = g\beta_T \Delta T d^3/\nu\alpha$ where ΔT is the horizontal temperature difference) simply consists of a single horizontally elongated unicellular flow (with

fluid moving upward in proximity to the heated wall, flowing along the upper wall from the right side to the left side, sinking when it meets the left (cold) wall and finally returning to its original position along the bottom).

Given the complexity of the matter, we are forced to articulate the presentation and discussion of the results in two main stages. More precisely, first we concentrate on 2D findings as a first necessary step to clarify the general problem relating to the existence of multiple solutions and transition to time dependence. Then the treatment is extended to fully 3D configurations.

2.2.1. The Zoo of 2D Modes

In this section, entirely devoted to the discussion of 2D results, two specific values of the aspect ratio A_x are considered for a representative small value of the Prandtl number (Pr = 0.01), namely $A_x = 4$ (already extensively investigated in past studies on the subject due to its relevance to typical industrial techniques for crystal growth) and $A_x = 10$. Moreover, the other parameter of interest, i.e., the compression (or expansion) ratio is varied in a relatively wide range ($0.1 \leq \eta \leq 10$) and the system response is described with respect to the Rayleigh number spanning two orders of magnitude, i.e., $O(10^3) \leq Ra \leq O(10^4)$.

The different results pertaining to this set of parameters for the case $A_x = 4$ can be seen in Figure 8, where the solutions have been reported as a function of η and arranged accordingly as 'columns', while the 'rows' correspond to variations in the value of Ra. By taking a look at this map, it becomes evident that, though the flow is forced to remain two-dimensional, a variety of solutions are allowed. These can be categorized as: (i) unicellular steady states (US), (ii) multi-roll steady states (MS), (iii) quasi-stationary states with weakly oscillating rolls (QS), (iv) 'classical' oscillatory rolls (with slender 'appendages' undergoing a kind of rhythmic displacement) (P), (v) states with periodically touching or 'kissing' rolls (K), (vi) regimes with periodically coalescing rolls (C), (vii) purely travelling waves (TW), (viii) mixed states (PLT) with travelling waves 'locally' modulated by roll pulsations or splitting behaviors (Lappa and Ferialdi, 2017).

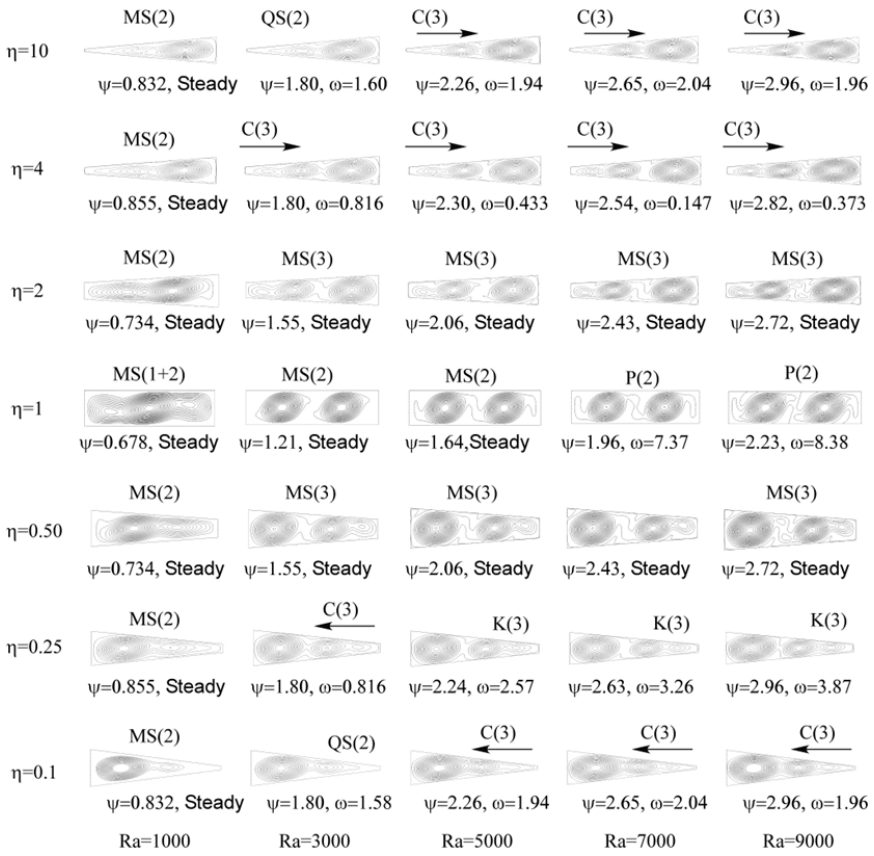

Figure 8. Map of solutions versus the parameter η and the Rayleigh number ($Ra = g\beta_T \Delta T d^3/\nu\alpha$) for $A_x = 4$ (ψ is the maximum of the streamfunction, multiple states existing for a fixed value of η have been reported as separate "rows" at the related value of η and its reverse).

While unicellular states obviously correspond to the trivial solutions for which the flow behaves as the classical circulation with opposing direct and return flows theorized by Hadley (1735), the other solutions relate to unstable states produced by the onset and development of hydrodynamic

disturbances (as explained before, hydrothermal waves are obviously suppressed in this case, given the absence of the third dimension).

As expected, the emerging flow is steady for relatively small values of the Rayleigh number and it becomes oscillatory as Ra is increased (as witnessed by the value of the angular frequency ω reported next to the maximum value of the streamfunction for each case).

Prior to embarking into an exhaustive description of these oscillatory states, in the following first we provide some initial and fundamental information on the *spatial symmetry properties* displayed by the flow (this strategy will prove very useful later when we will discuss the general features of such solutions from a temporal point of view and focus on the emergence of hybrid states and related dynamics).

By carefully inspecting Figure 8, the reader will realize that the behaviors observed for a given η (e.g., η = 2) are the "mirror image" of those seen for its inverse value (η = 0.5). The number of rolls and their morphological properties are essentially the same. As an example, the rolls structures obtained for η = 2 could formally be turned into those emerging for the same value of the Rayleigh number and η = 0.5 by simply rotating the overall system by 180°. By swapping the cold side and the hot side, indeed, such a rotation would transform the initial problem with η > 1 and gravity directed downwards (where the fluid raises along the sidewall of larger size, namely the hot wall located on the right of the figure) into a completely equivalent problem for η < 1 in which gravity is directed upwards and the fluid moves in the same sense (upwards) in proximity to the cold side (the cold side being located on the right side after the 180° rotation). In Lappa and Ferialdi (2017), this property of the velocity field for η ≠ 1 was named the "*180°-rotation invariance principle after η reversal*". From a mathematical standpoint such a property may be formalized as follows (the tilde being used to indicate the transformed quantities):

$$\begin{bmatrix} \widetilde{u} \\ \widetilde{v} \end{bmatrix}_{\eta} = \underline{\underline{R}}(180°) \begin{bmatrix} u \\ v \end{bmatrix}_{1/\eta} \tag{5a}$$

with the rotation matrix defined as

$$\underline{\underline{R}}(\theta) = \begin{bmatrix} \cos\theta & -\sin\theta \\ -\sin\theta & \cos\theta \end{bmatrix} \tag{5b}$$

In particular, the cases $\eta = 1$ might be seen as special conditions for which the "*180°-rotation invariance principle after η reversal*" would reduce to the "*central symmetry*" already discussed with regard to the examples shown in Figure 7.

Having provided a general characterization of the flow from a spatial perspective, we now turn to describing in detail the related temporal dynamics. The typical oscillatory behavior for the special condition $\eta = 1$ can be seen in Figure 9 for Ra = 9000. In agreement with earlier numerical studies about rectangular cavities, flow oscillations manifest as morphological variations periodically affecting the shape of the peripheral streamlines of each roll ((P)-mode).

As shown in Figure 8, for $A_x = 4$, this kind of oscillatory flow is still possible if values of η in a given neighbourhood of $\eta = 1$ are considered ($0.75 \leq \eta \leq 1.33$). In particular, for $\eta = 0.75$ ($\eta = 1.33$) and $\eta = 0.65$ ($\eta \cong 1.5$) oscillations of the P type are excited for Ra $\geq$ 7000 and Ra $\geq$ 9000, respectively.

Moreover, though the system experiences a strong stabilization in the ranges $0.4 \leq \eta < 0.75$ and $1.33 < \eta \leq 2.5$, oscillatory behaviors are again possible for both $\eta < 0.4$ or $\eta > 2.5$. Interestingly, Lappa and Ferialdi (2017) identified transition to time dependence in these ranges of η for relatively small values of Ra (hereafter, for simplicity we will discuss the behaviors for $\eta < 1$, as those for $\eta > 1$ can be easily gathered by applying the aforementioned invariance principle).

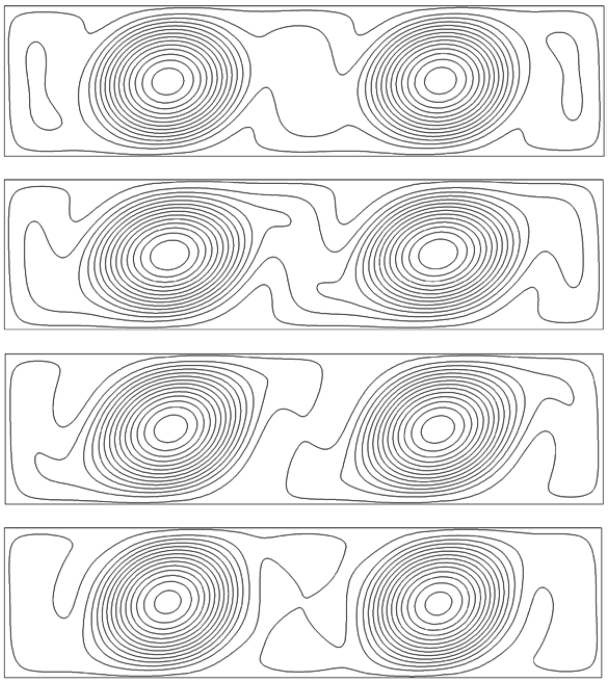

Figure 9. Oscillatory flow of the (P) type for $A_x = 4$, $\eta = 1$ and Ra = 9000: four snapshots equally spaced within one period of oscillation.

In the intervals ($0.2 \leq \eta \leq 0.3$) and for $Ra \geq 3000$, in particular, through systematic variation of the initial conditions and/or the use of different schemes for the integration of the overarching equations, Lappa and Ferialdi (2017) identified *two different kinds of solutions coexisting in the space of parameters*, namely states pertaining to the (K) or (C) regime (relevant examples being shown in Figures 10 and 11, respectively).

In the first case, two of the tree rolls existing at the same time in the cavity (more precisely, the central roll and the roll near the shortest wall) display a weakly oscillatory process in which one of them contacts periodically its neighbor ("kissing" rolls behavior, which provides a justification for the "K" letter to label it) whereas the third roll remains steadily located in proximity to the left (cold) wall as a separate entity.

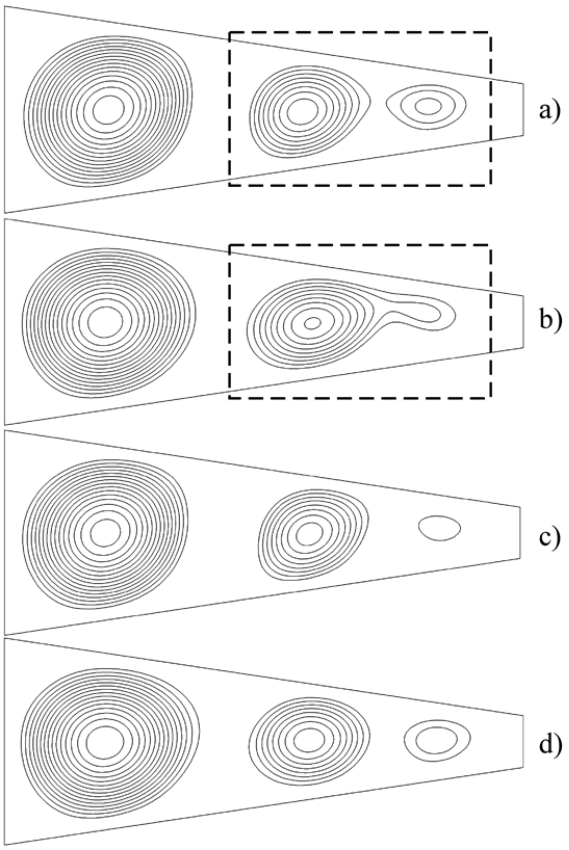

Figure 10. Oscillatory flow of the (K) type for $A_x = 4$, $\eta = 0.25$ and Ra = 9000: four snapshots equally spaced within one period of oscillation.

The kissing behavior, however, is replaced by a complete roll coalescence process as solutions pertaining to the (C) branch are considered (Figure 11). The roll merging mechanism takes place essentially in the left part of the cavity as a result of the displacement of the roll initially located in the center of the cavity towards the longest vertical wall. As soon as the central and left rolls become a single entity, a new roll emerges at the right side thereby preserving the initial number of rolls and giving the observer the feeling of a *disturbance that spreads continuously from the right side to the left side* (i.e., in the direction of growing cross-sectional area). Lappa and Ferialdi (2017) found this

alternate mode of convection, featured by the propagation of a disturbance from regions of reduced cross-sectional area towards regions where the cavity is thicker, to be *the preferred mode of oscillatory instability* in the end regions of the considered interval of η (namely when η is very small or very large). Notably, Lappa and Ferialdi (2017) also highlighted that such a travelling disturbance or wave (TW) can become the dominant mechanism of oscillatory convection through the entire range of Rayleigh numbers and values of $\eta \neq 1$ if cavities with larger aspect ratio A_x are considered.

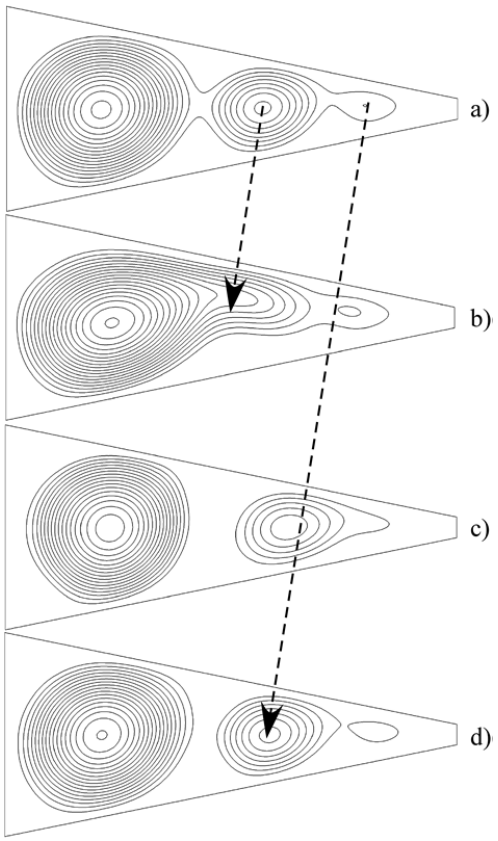

Figure 11. Oscillatory flow of the (C) type for $A_x = 4$, $\eta = 0.1$ and $Ra = 9000$: four snapshots equally spaced within one period of oscillation.

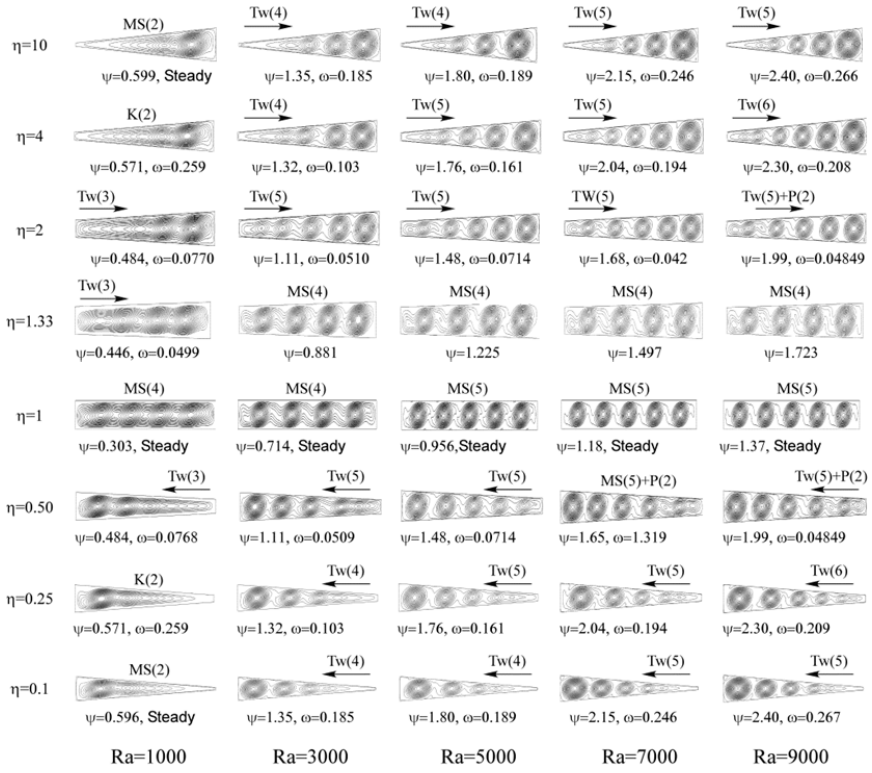

Figure 12. Map of solutions versus the parameter η and the Rayleigh number ($Ra = g\beta_T \Delta T d^3/\nu\alpha$) for $A_x = 10$ (ψ is the maximum of the streamfunction, multiple states existing for a fixed value of η have been reported as separate "columns" at the related value of η and its reverse).

Related results, summarized in Figure 12 for $A_x = 10$ using the same mode of representation already considered for Figure 8, indeed, provide evidence for such a general scenario (together with some interesting information about 'variants' and mixed states, which emerge for specific couples (η, Ra)).

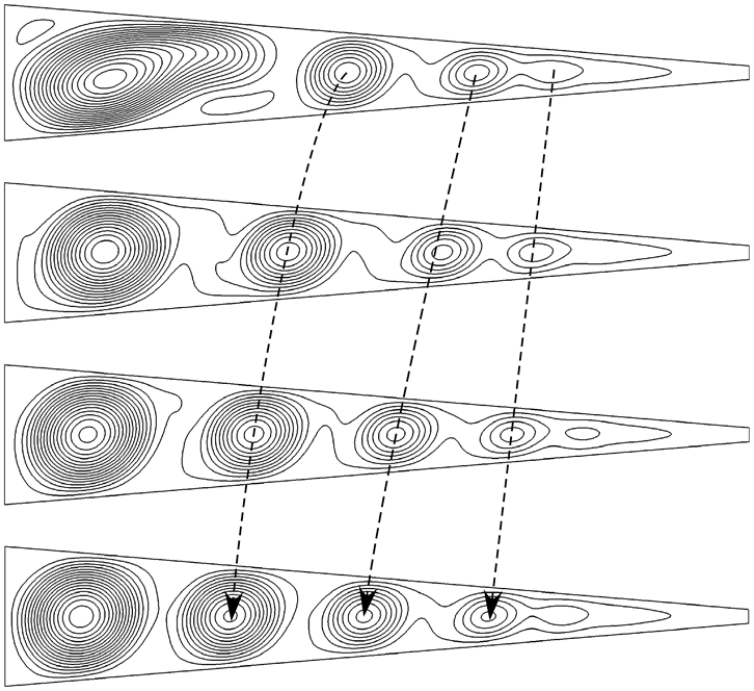

Figure 13. Oscillatory flow for $A_x = 10$, $\eta = 0.1$ and Ra = 9000: four snapshots equally spaced within one period of oscillation.

As an example, for $A_x = 10$, $\eta = 0.1$ or $\eta = 10$, the initially steady unicellular flow obtained for Ra = 1000 and 2000 is quickly replaced on increasing Ra by an oscillatory mode of convection with the disturbance always clearly travelling in the direction in which the cross-section of the domain increases, namely from the hot wall to the cold wall for converging walls and in the *opposite direction* in the case of diverging walls.

As shown in Figure 13, the oscillatory disturbance manifests itself as a well-defined chain of cells moving from the thinnest side towards the thickest one, with the exception of an almost motionless roll steadily located in proximity to the target wall, regardless of whether $\eta < 1$ or $\eta > 1$ (the stable behavior of such a stationary roll being supported by the relatively strong buoyancy forces being present in the thicker part of the domain).

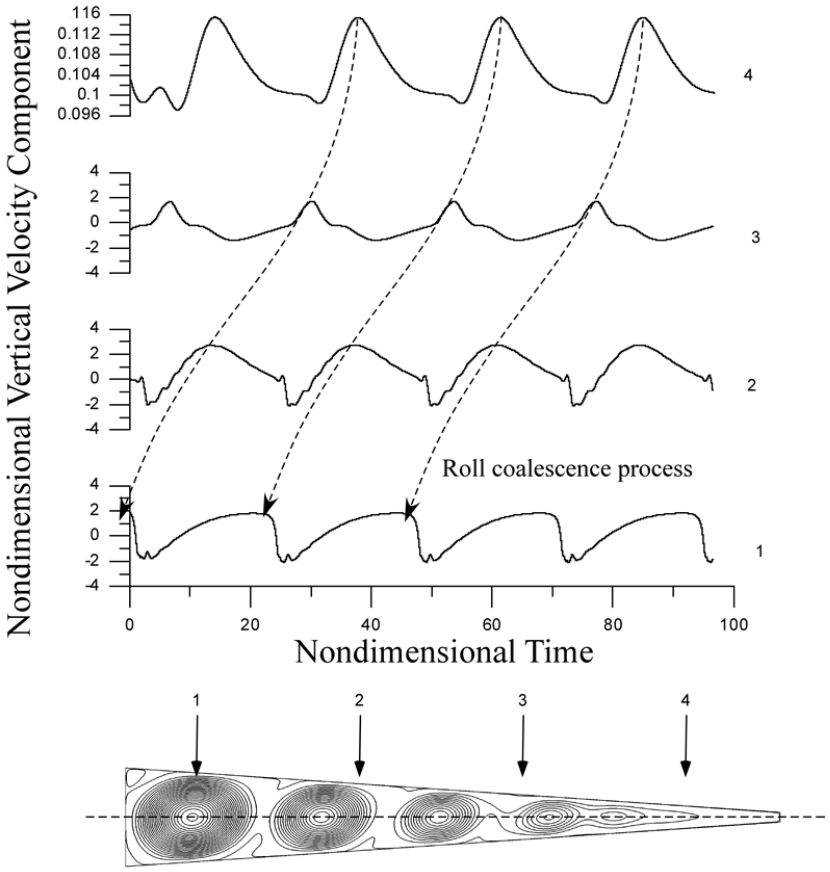

Figure 14. Velocity signals as measured by four probes periodically positioned along the horizontal direction ($A_x = 10$, $\eta = 0.1$ and $Ra = 9000$, vertical velocity at $y = 0$). The modulation of the sinusoidal signals being related to the main frequency is due to the presence of a second frequency for this relatively high value of the Rayleigh number.

As soon as one of the travelling rolls meets this roll, they merge. As already explained for the cavity with $A_x = 4$, when such a coalescence process is completed, a new roll emerges near the other sidewall, thereby *keeping constant the average number m of convective cells affecting the cavity at any instant* (and preserving the time periodicity of the overall process).

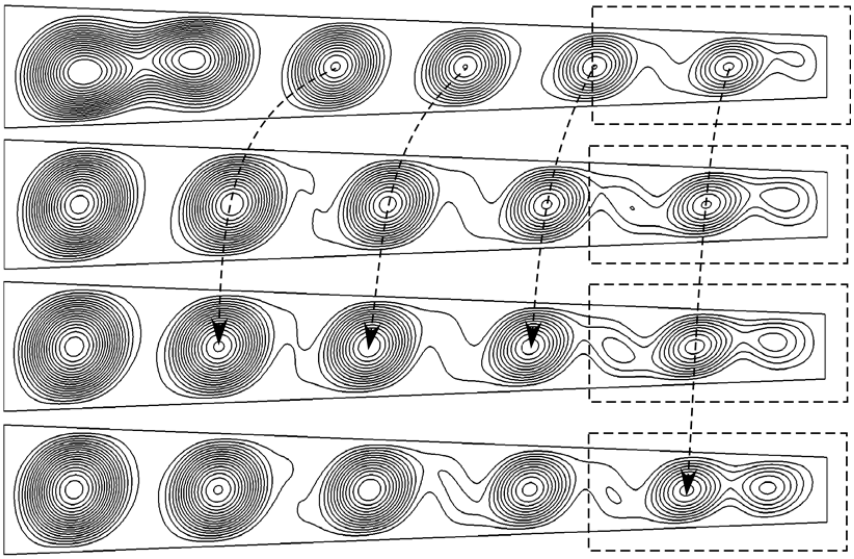

Figure 15. Oscillatory flow for $A_x = 10$, $\eta = 0.5$ and Ra = 9000: four snapshots equally spaced within one period of oscillation.

Interestingly, the velocity of propagation of the rolls is not constant along the x axis, as witnessed by the signals provided by a set of probes evenly spaced along this axis (Figure 14). Apart from confirming the travelling nature of the disturbance, made evident by the continuous phase shift displayed by the signals measured at different locations, this plot clearly shows that a moving roll experiences a varying velocity in the course of its migration.

For $A_x = 10$, Lappa and Ferialdi (2017) found the scenario for $\eta = 0.25$ and $\eta = 4$ to be very similar to that for $\eta = 0.1$ and $\eta = 10$, respectively. Nevertheless, some interesting dynamics were spotted for $\eta = 0.5$ ($\eta = 2$). According to their findings, indeed, for these values of η and relatively high values of Ra (Ra≥7000), a localized disturbance can manifest in the form of a modulation affecting the thinnest part of the cavity (highlighted by the dashed rectangle in Figure 15).

The localized oscillatory behavior is essentially due to the time-periodic formation of a three-roll structure in the right part of the physical domain (Figure 15). Apparently, this structure (resembling the ‘twisted’

convective structure encapsulating the three co-rotating vortices shown in Figure 6a for the purely rectangular cavity with $A_x = 4$ and $Ra = 10^3$) derives from the 'splitting' of the original roll located near the right wall (this is why this state was referred to by Lappa and Ferialdi (2017) as an m = "5+2" mode). For Ra = 9000, interestingly, this localized perturbation can exist in parallel with the travelling wave, thereby giving rise to a regime with two coexisting frequencies (one relatively small connected to the wave and another much larger one accounting for the localized disturbance of the (P) type).

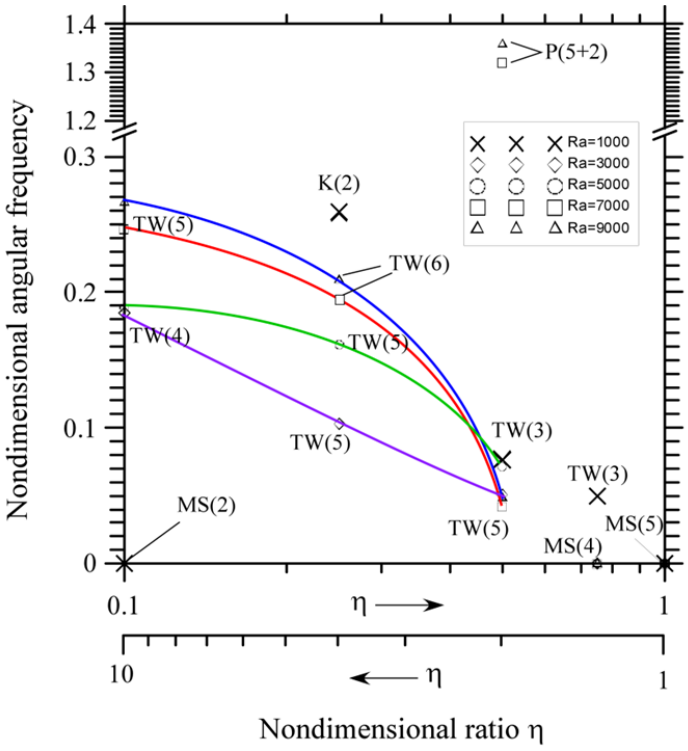

Figure 16. Oscillation angular frequency versus the expansion or compression rate η for $A_x = 10$ and different values of the Rayleigh number (for η = 1, transition to oscillatory flow occurs for Ra = 14500 with angular frequency $\omega \cong 6.48$, not shown in this figure).

If η is made $\cong 1$, all these waveforms and related modulations effects are finally replaced by a completely different time-dependent scenario where travelling disturbances are no longer a feature of the flow (the spatio-temporal behavior becoming similar to that reported in Figure 9 for $A_x = 4$, $\eta = 1$ and $Ra = 9000$).

One may therefore state that, taken together, Figures 12 and 16 indicate that TW branches are dominant in the 'external regions' of the η-interval ($\eta \leq 0.5$ and $\eta \geq 2$); and that, an increase in the Rayleigh number generally causes a shrinkage of the effective η intervals in which (TW) disturbances are allowed. The latter observation is in line with the scenario already described for $A_x = 4$ (see Figure 8), that is, the preferential mechanism of oscillations is gradually transferred from low-frequency waves to high-frequency disturbances of the (P) type when Ra is increased (Lappa and Ferialdi, 2017).

2.2.2. The Zoo of 3D Modes

Having finished a description of the 2D flow in enclosures with converging or diverging walls, we turn now to considering the role played by the third dimension, i.e., the dynamics in systems spatially extended along the spanwise direction z. These cases clearly display an increased degree of complexity with respect to 2D solutions as hydrodynamic modes can no longer be an exclusive feature of the emerging flow. Shear-driven modes can indeed be completely replaced by hydrothermal modes or still be present and interact with them, leading to a variety of possible scenarios depending on the effective circumstances considered.

As in the presence of complex dynamics, in order to make the discussion simpler and clearer, a reduction of the considered ranges of parameters is beneficial, in this section we will limit ourselves to considering configurations with $A_x = 10$.

Let us recall that, as illustrated at the beginning of this chapter (Sects. 1.1 and 1.2), in past linear stability analyses based on the assumption of horizontal parallel flows, hydrodynamic and hydrothermal disturbances were observed as the preferred perturbations for $Pr = O(10^{-2})$ and $Pr = O(10^{-1})$, respectively (see Figure 3). More precisely, Hart (1983) found the

hydrodynamic and hydrothermal disturbances to be the most dangerous for $Pr < 0.015$ and $0.015 < Pr < 0.27$, respectively. Kuo and Korpela (1988) slightly revised these ranges as $Pr < 0.033$ and $0.033 < Pr < 0.2$ (the critical curves for these two different categories of disturbances were also found to be relatively close one to another in terms of values of the Rayleigh number, the reader being referred once again to Figure 3). The influence of the system inclination on the (codimension-two) point, where the branches pertaining to the different disturbances intersect, was investigated by Delgado-Buscalioni (2001), who confirmed the existence of this point at $Pr \cong 0.03$ for purely horizontal cavities, showing that it moves towards smaller values of Pr as soon as the considered configuration undergoes a *net* tilt.

As the last part of this chapter is explicitly devoted to the examination of these fundamental modes of convection in 3D geometries, we therefore focus on two representative values of the Prandtl number located in the ranges reported above, i.e., $Pr = 0.01$ and $Pr = 0.05$. In particular, to facilitate direct comparison with the results obtained under the constraint of two-dimensionality, first we describe the emerging dynamics for the same value of the Prandtl number (i.e., $Pr = 0.01$) already examined in Sect. 2.2.1.

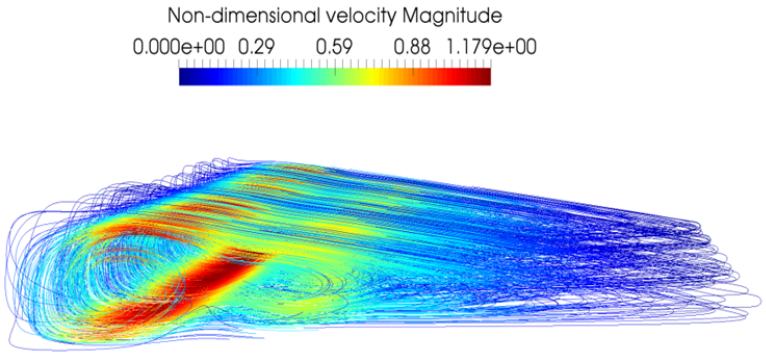

Figure 17. Steady base flow in different sections along the z direction ($A_x = 10$, $\eta = 0.1$, $A_z = 10$, periodic boundary conditions along z, $Pr = 0.01$, $Ra = 1000$, $Gr = Ra/Pr = 10^5$).

As a first example, Figure 17 shows the 3D field emerging for Ra = 1000 assuming $A_z = 10$, $\eta = 0.1$ and periodic boundary conditions along the z axis.

In agreement with the 2D findings (Figure 12), it can be seen that for this value of the Rayleigh number, a second circulation nucleates in the original unicellular structure and the overall flow is steady.

When Ra is increased, however, interesting departures from 2D behaviors occur.

A first evidence of such a departure is immediately provided by Figure 18, where we have reported the velocity field for Ra = 2000. By careful inspection of these plots, indeed, the reader will realize that interesting flow features along the spanwise direction z can be detected. These consist of four peaks of velocity (red arrows) located in proximity to the thickest side of the cavity. Evidence for the essentially 3D nature of the flow is also reinforced by the presence of recognizable vortices spatially extended throughout the xz plane. Moreover, this flow is essentially oscillatory.

The difference with respect to the 2D flow reported in Figure 12 becomes even more evident if one considers that, on the basis of the study conducted under the constraint of two-dimensionality, the solution should still be steady for $A_x = 10$, $\eta = 0.1$ and Ra = 2000. According to the 2D study, time-dependence should enter the dynamics at $Ra \cong 3000$ in the form of a wave (TW) with four rolls travelling in the streamwise direction (Figure 12). In the present case, apart from the second roll being embedded in the general circulation (Figure 18a), no other convective features are visible in the transverse (xy) plane. Important differences also concern the intrinsic oscillatory nature of the flow. The recognizable convective vortices in the xz plane (Figure 18b) do not travel along the positive or negative z direction (as one would expect for a travelling wave); rather they assume the typical behavior of a standing wave, that is, the disturbances continuously oscillate between two limiting positions along the z-axis.

Given the considered value of the Prandtl number (Pr = 0.01) and the relatively low magnitude of the Rayleigh number for which transition to time-dependent flow occurs (Ra appreciably smaller than that required to

excite hydrodynamic disturbances in the equivalent 2D case), these simple observations naturally lead to a fundamental question, that is, discerning the nature of the observed (3D) disturbances (Figure 18c).

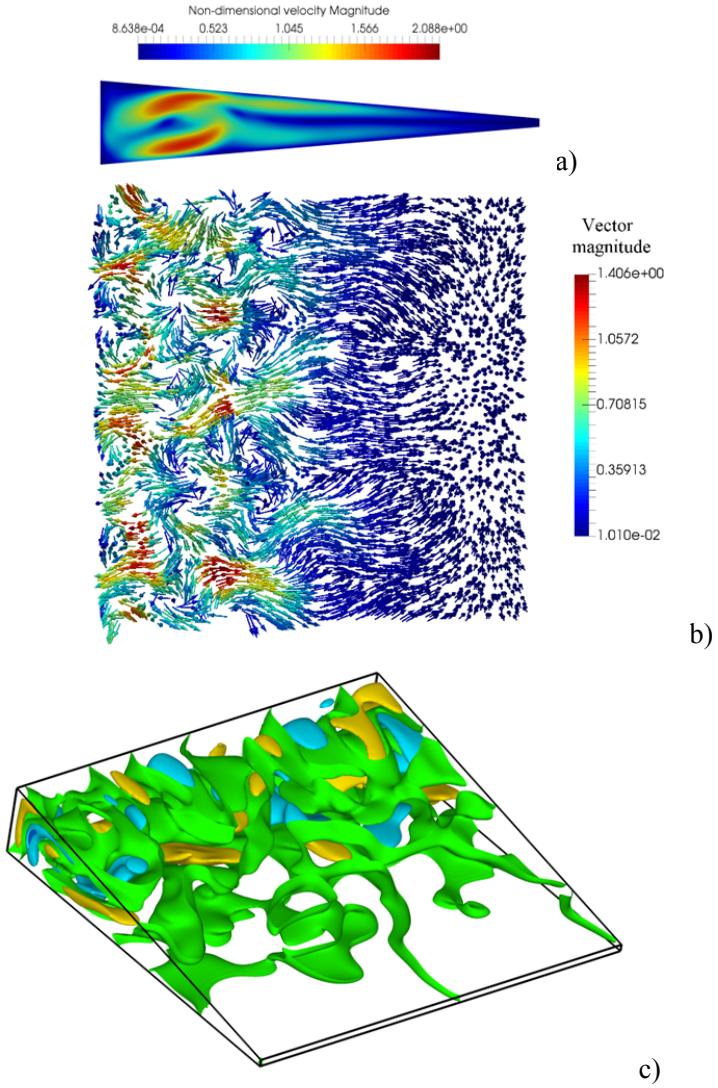

Figure 18. Snapshots of 3D oscillatory flow for Pr = 0.01, A_z = 10 (periodic boundary conditions, initial conditions corresponding to a quiescent thermally diffusive state), Ra = 2000 (Gr = $2x10^5$): a) velocity distribution in the xy plane, b) Velocity vector plot in the xz mid-plane, c) isosurfaces of the *w* (along z) component of velocity.

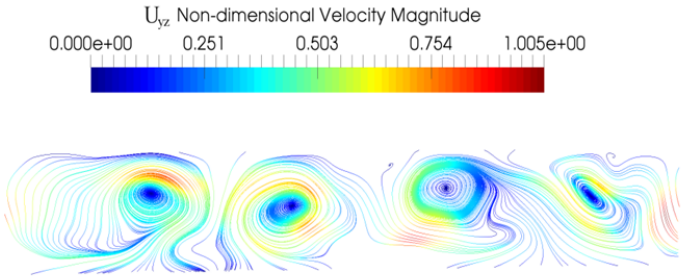

Figure 19. Projection of the velocity field in the yz plane at x = 1/8A_x (Pr = 0.01, A_x = 10, A_z = 10, periodic boundary conditions, Ra = 2000, temperature equation uncoupled).

Resolving this question, however, is not straightforward as one would imagine as it requires separating different contributions, which are generally intertwined.

Interestingly, Lappa and Ferialdi (2018b) showed that direct numerical solution of the overarching eqs. (1)-(3) (Sect. 1.3) can still be used as a valid tool to get meaningful information on these phenomena provided it is used in combination with specific rational arguments about the hydrodynamic and hydrothermal fundamental modes of instability and related differences (see again Sects. 1.1 and 1.2).

More precisely, they elaborated a specific analysis strategy based the possibility to uncouple the energy and momentum equations (solving the balance equations for mass and momentum only while assuming a fixed thermally diffusive distribution for the temperature).

The physical reasoning underpinning this approach can readily be understood by taking into account that the simple action of preventing the temperature field from developing changes should impede the onset and ensuing growth of any disturbance of hydrothermal nature.

The outcomes of such simulations for the same conditions considered for Figure 18 (shown in Figure 19) reveal that, as four longitudinal rolls (with axes parallel to the applied temperature gradient, i.e., oriented along the x axis) are still present (and since any processes that depend on the amplification of the aforementioned helicoidal disturbances are excluded in this case), the oscillatory dynamics reported in Figure 18 must therefore be

considered of a hydrodynamic nature (which is relatively an unexpected result if one considers that hydrodynamic modes are generally thought of as purely two-dimensional disturbances).

Interestingly, Lappa and Ferialdi (2018b) could even track precisely the process leading from the initial steady state shown in Figure 17 to the much more involved situation evident in Figure 18 through evaluation of the so-called *correlation dimension*, which can generally be regarded *as a measure of the degrees of freedom possessed by a system*.

A rigorous definition of this quantity can be found in the literature where it is introduced as a generalization of the classical concept of dimension of a subset of the Euclidean space. While the dimension of a subset of the Euclidean space can be seen as the number of parameters needed to locate precisely a generic point of the set, the correlation dimension somehow accounts for the rate with which the typical 'orbit' (described by a system in the space of phases) 'visits' different parts of an attractor (Grassberger, 1983). Most remarkably, this percentage can take non-integer values. Following Balatoni and Renyi (1956), assuming the phase space to be partitioned via a grid of cubes *C* having characteristic size r (side length), the correlation dimension can formally be expressed as:

$$\mathcal{D}_2 = \lim_{r \to 0} - \frac{\ln\left\{\sum_j \left[\tau(C_j)\right]^2\right\}}{\ln(r^{-1})} \tag{6}$$

where C is the generic cube with side having length r in the phase space, $\underset{\sim}{\zeta}(\underset{\sim}{\zeta}_o,t)$ is the orbit originating from a generic initial condition $\underset{\sim}{\zeta}_o$, and $\tau(C, \underset{\sim}{\zeta}_o,\Delta t)$ formally represents the percentage of time that $\underset{\sim}{\zeta}(\underset{\sim}{\zeta}_o,t)$ spends in C in a time interval Δt (Lappa, 2009). Over the years, algorithms able to provide an estimate of this quantity have been conceived, a relevant example being represented by the procedure defined by Grassberger and Procaccia (1983ab).

This dimension is generally regarded as an effective measure of the number of 'active modes' in a dynamical system (Theiler, 1986). Its values

computed with the algorithm by Grassberger and Procaccia (1983ab) for the cavity shown in Figure 18 and magnitudes of the Rayleigh number progressively increasing from 1000 towards 2000 are reported in Figure 20, from which the reader will realize how quick the progression towards chaotic features can be in such a restricted interval of the control parameter when the flow is allowed to be 3D.

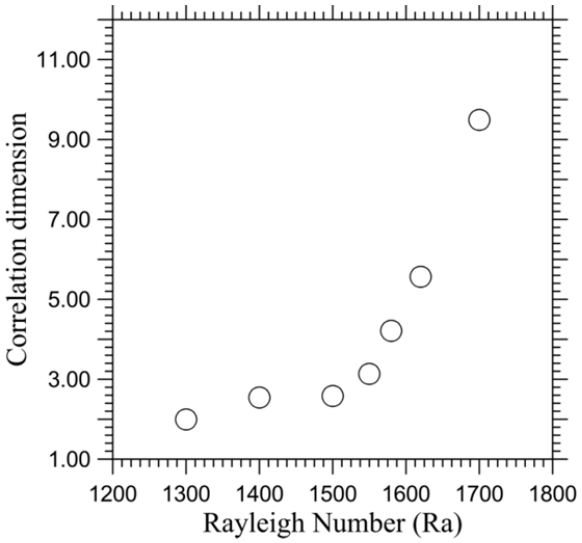

Figure 20. $\mathcal{D}_2$ versus Rayleigh number (Pr = 0.01, A_x = 10, A_z = 10, η = 0.1, periodic boundary conditions).

More precisely, as soon as Ra becomes larger than 1550, $\mathcal{D}_2$ exceeds 3 ($\mathcal{D}_2 \cong 3.14$ for Ra = 1550, $\mathcal{D}_2 \cong 4.22$ for Ra = 1580) and then suddenly increases for higher values of Ra. Such a gain in chaotic features can clearly be interpreted as the quick development of high-dimensional chaos. The reader may come to the same conclusion by taking a look at Figure 21 (showing the sequence of 'signals' for increasing values of Ra) or directly at the frequency spectra reported in Figure 22 for Ra = 2000. The latter figure is particularly meaningful as it provides immediate evidence for the rather *turbulent nature* of the 3D flow established for small values of the

Rayleigh number when the dominant disturbances are hydrodynamic. This should be regarded as another important distinguishing mark with respect to the 2D solutions.

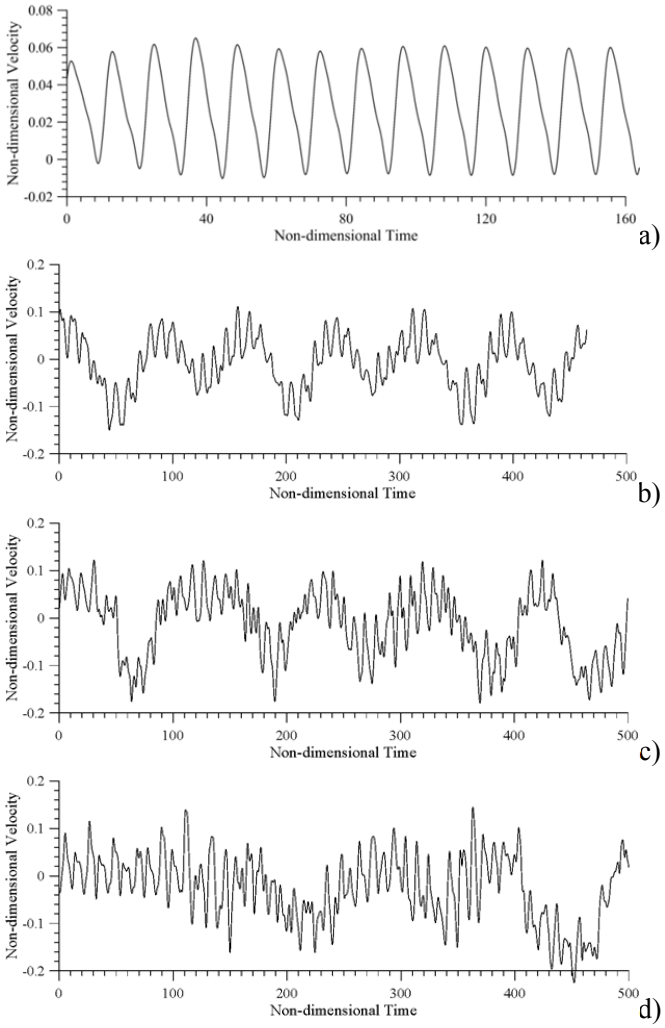

Figure 21. Velocity signals measured by a numerical probe located at a fixed point ($x = 3/8A_x$, $y = 0$, $z = A_z/2$) for $Pr = 0.01$, $A_x = 10$, $A_z = 10$, $\eta = 0.1$, periodic boundary conditions and different values of the Rayleigh number: a) $Ra = 1400$, b) $Ra = 1500$, c) $Ra = 1620$, d) $Ra = 1700$.

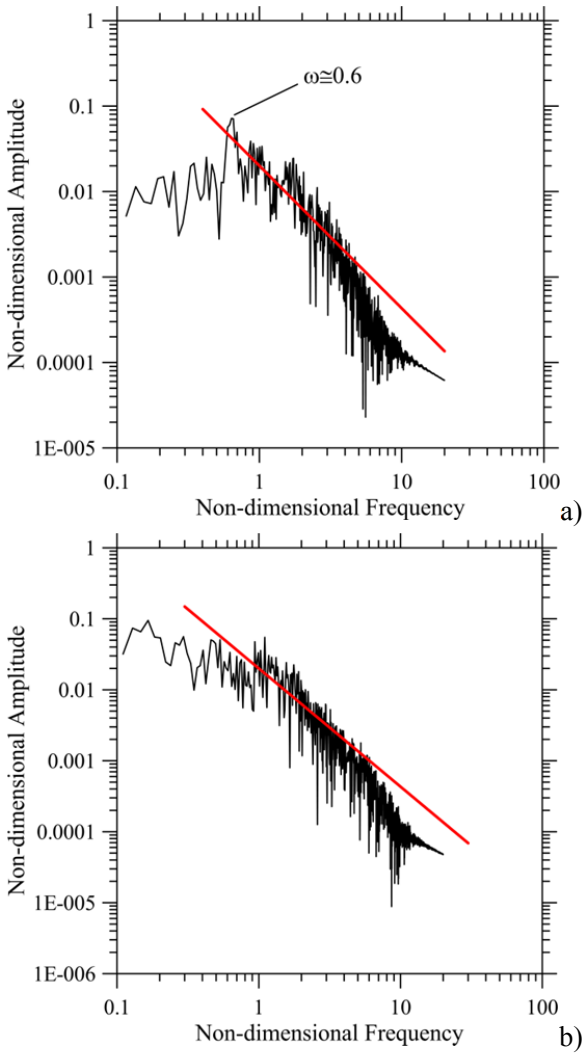

Figure 22. Non-dimensional velocity amplitude as a function of the non-dimensional frequency (Pr = 0.01, A_x = 10, A_z = 10, η = 0.1, periodic boundary conditions, Ra = 2000, Gr = $2x10^5$): a) temperature equation coupled (mixed regime with dominant hydrodynamic modes and OLR with ω ≅ 0.6), b) temperature equation uncoupled (purely hydrodynamic oscillatory mode of convection).

As discussed in Sect. 2.2.1, under the constraint of two-dimensionality (Figure 12) the flow retains an essentially laminar behavior. For instance,

even for Ra = 9000 the velocity field cannot be considered turbulent as its frequency spectrum is limited to the presence of one or two incommensurate frequencies only. This behavior is in evident contrast with the scenario presented in Figure 22, where complex multimodal temporal dynamics can be seen even if the Rayleigh number is as small as 2000. The high-dimensional nature of the chaos relating to this state is confirmed by the fact that the spectra shown in such figure are in line with the typical behavior originally theorized by Kolmogorov (1941abc, 1942) about the development of isotropic turbulence. In order to make this specific aspect evident, following the same approach used by De et al. (2017), we have reported the frequency and related amplitude in Figures 22 using logarithmic scales for the axes and comparing the resulting diagram with a power law $P(\omega) = (\omega/\omega_c)^{-s}$ (where ω_c is a fitting parameter).

It can be seen that the frequency spectrum of velocities aligns perfectly with the $\omega^{-5/3}$ law in a wide interval of frequencies, as envisaged by the aforementioned Kolmogorov's turbulence similarity hypothesis. The related set of scales, also known as 'inertial range' corresponds to the so-called *energy cascade process* by which the directional biases of the large length scales are lost as energy is transferred to increasingly smaller scales. Such an interval is limited at one side by the typical length-scale L of the cavity, which is the scale at which energy is injected into the fluid via the action of buoyancy forces and at the other side by the scale where internal energy is produced by frictional effects at expenses of the kinetic energy of the flow.

Though, as illustrated in the preceding text, some interesting conclusions might be gathered from a careful comparison of 2D and 3D results, the variety of possible situations, however, can even be richer than what we have just discussed if the Prandtl number is allowed to change. According to numerical simulations (see again Lappa and Ferialdi, 2018b), indeed, an increase in the Prandtl number to Pr = 0.05 while keeping all the other parameters unchanged (A_x = 10, A_z = 10, periodic boundary conditions, Ra = 2000) can alter significantly the emerging dynamics. As evident in Figure 23, for such conditions, the pattern becomes much more

regular in space. Moreover, the disturbances behave as *a wave travelling along the z direction* (Figure 24).

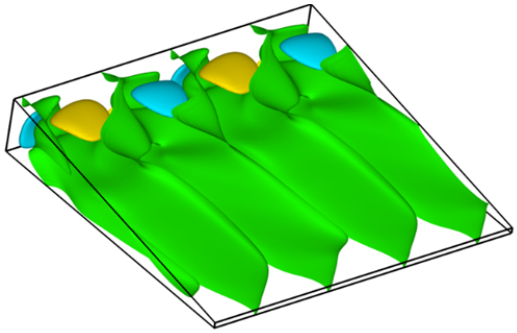

Figure 23. Isosurfaces (snapshot) of the *w* component of velocity (Pr = 0.05, A_x = 10, A_z = 10, η = 0.1, periodic boundary conditions, initial conditions corresponding to a quiescent thermally diffusive state, Ra = 2000, Gr = $4x10^4$, OLR mode).

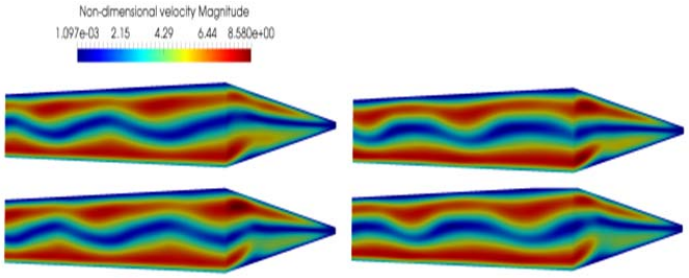

Figure 24. OLR mode (Pr = 0.05, A_x = 10, A_z = 10, η = 0.1, periodic boundary conditions, Ra = 2000, Gr = $4x10^4$): four snapshots of non-dimensional velocity magnitude evenly distributed in time are shown (OLR with nondimensional angular frequency 2.81).

Simulations repeated after disabling the solution of the temperature equation (yet to exclude any disturbance of thermal buoyancy origin) have clearly indicated that the emerging solution can be regarded as an OLR mode as it *cannot survive after equation uncoupling*.

The outcomes of this study are summarized in Figures 25, which together with Figure 22, provide the spectrum of frequencies for the different situations examined so far, namely Pr = 0.01 (A_x = 10, A_z = 10 with periodic boundary conditions along z, η = 0.1) with the energy equation and the Navier-Stokes equations coupled and uncoupled (Figure

22a and 22b, respectively) and the analogous spectra for the case with Pr = 0.05 (Figures 25a and 25b).

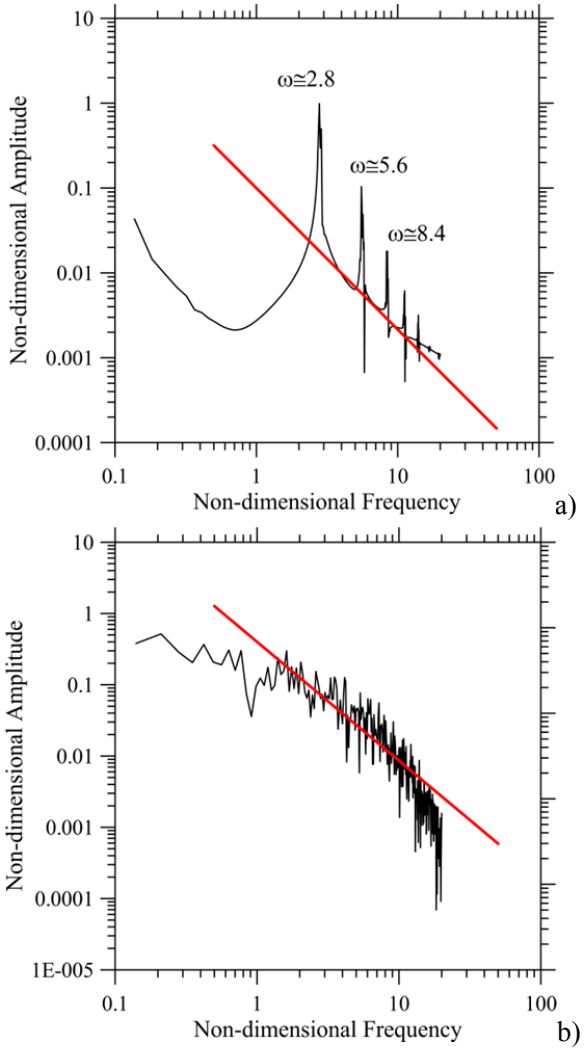

Figure 25. Non-dimensional velocity amplitude as a function of the non-dimensional frequency (Pr = 0.05, A_x = 10, A_z = 10, η = 0.1, periodic boundary conditions, initial conditions corresponding to a quiescent thermally diffusive state, Ra = 2000, Gr = $4x10^4$): a) temperature equation coupled (OLR mode), b) temperature equation uncoupled (hydrodynamic oscillatory mode of convection).

In particular, Figure 25 reveals that if, for Pr = 0.05, the onset of OLR modes is prevented by uncoupling the equations, the spectrum of frequencies takes the same complex structure obtained for Pr = 0.01 for the case of hydrodynamic disturbances.

Comparison between Figures 22a and 22b is also useful as it leads to the conclusion that though the spectrum retains a similar multi-frequency (broad-band) appearance when the temperature equation is switched off, the main peak visible in Figure 22a in the small-frequency region of the spectrum (around $\omega = 0.6$) disappears in Figure 22b, which should be regarded as a clear hint for the OLR nature of the perturbations being associated with it. Another interesting outcome of this figure is that it also definitely proves that hydrodynamic and OLR modes can *coexist*.

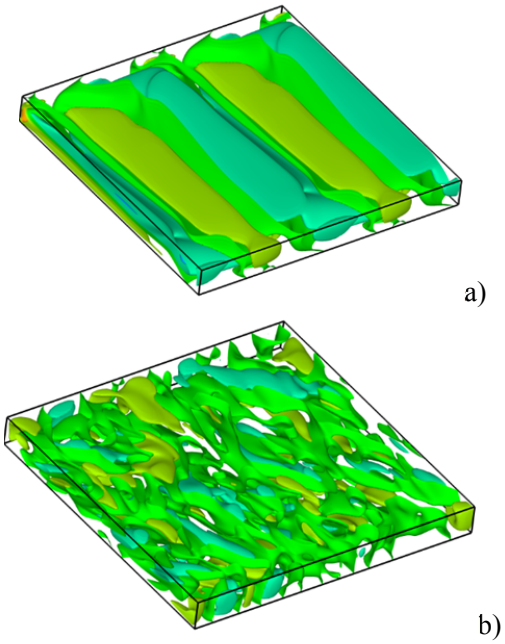

Figure 26. Isosurfaces (snapshot) of the w component of velocity (Pr = 0.05, $A_x = 10$, $A_z = 10$, $\eta = 1$, periodic boundary conditions, initial conditions corresponding to a quiescent thermally diffusive state, Ra = 2000, Gr = 4×10^4): a) temperature equation coupled (OLR mode), b) temperature equation uncoupled (hydrodynamic oscillatory mode of convection).

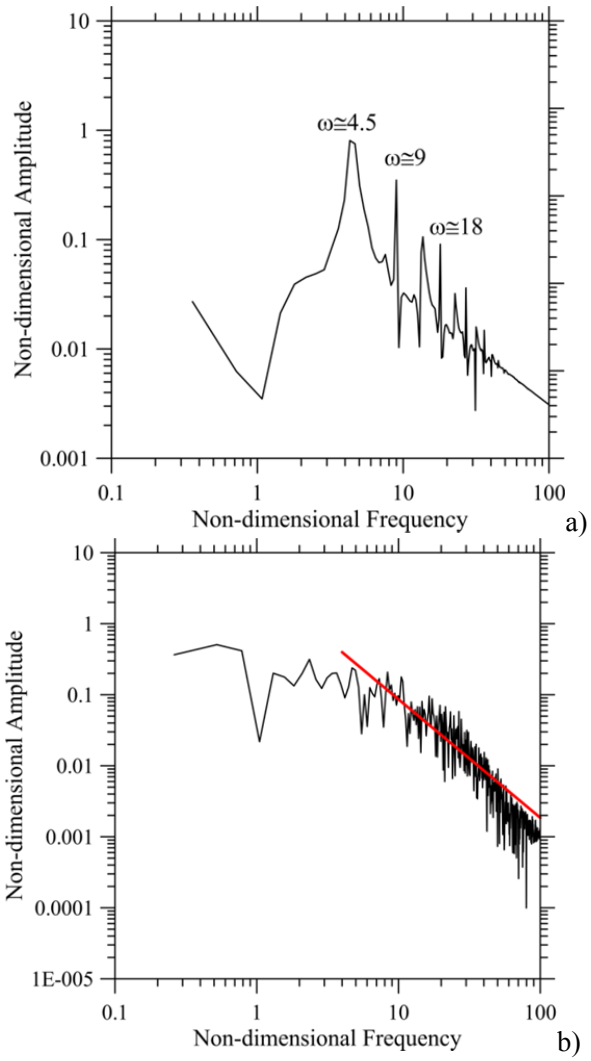

Figure 27: Non-dimensional velocity amplitude as a function of the non-dimensional frequency for the same conditions considered in Figure 26a and 26b, respectively.

The same conclusions could be drawn for the case with horizontal walls ($\eta = 1$, see Figures 26 and 27). The primary mode of convection is an OLR (Figures 26a and 27a) unless the energy equation is uncoupled (leading again to 3D hydrodynamic disturbances, Figures 26b and 27b).

Interestingly, cross examination of Figure 25a and 27a also indicates that the fundamental frequency of the OLR is slightly larger for the cavity with horizontal walls ($\omega \cong 2.8$ and $\omega \cong 4.5$ for $\eta = 0.1$ and $\eta = 1$, respectively).

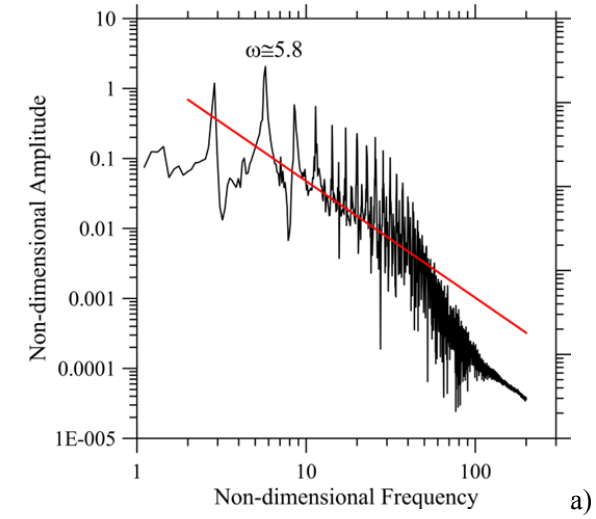

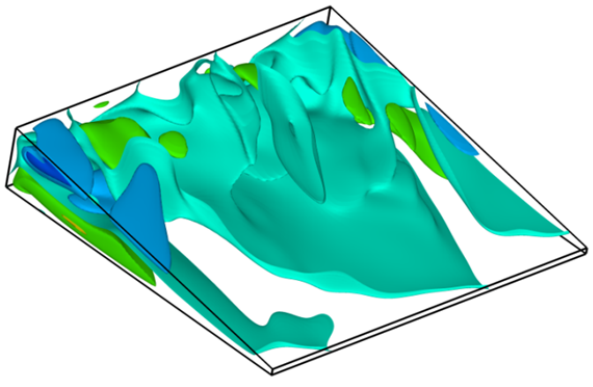

Figure 28. Properties of the oscillatory state for Pr = 0.05, $A_x = 10$, $A_z = 10$, $\eta = 0.1$, periodic boundary conditions, initial conditions corresponding to a quiescent thermally diffusive state, Ra = 10000 ($Gr = 2x10^5$, mixed regime with hydrodynamic and OLR modes): a) frequency spectrum, b) isosurfaces (snapshot) of the *w* component of velocity.

These observations naturally lead us to re-introduce another of the interesting aspects being associated with these dynamics, that is, the problem relating to the existence of multiple solutions (already discussed to a certain extent for the 2D flow in Sect. 2.2.1). Multiple solutions are still possible when the constraint of two-dimensionality is removed. As an example, for Pr = 0.05 Lappa and Ferialdi (2018b) clearly observed different states existing independently at $Ra = 2x10^4$.

Along these lines, yet for the case with converging walls and $\eta = 0.1$, Figure 28 shows the emerging flow (snapshot) and related frequency spectrum for Pr = 0.05 and $Ra = 10^4$ as a necessary pre-requisite to let the reader appreciate the multiple solutions that can be obtained when Ra is increased to $2x10^4$. For $Ra = 10^4$, a peak located at $\omega \cong 6$ in the left region (low-frequency interval) of the spectrum represents an OLR mode, while the right part (high-frequency interval) closely resembles that found for the case of dominant hydrodynamic disturbances. Therefore, this figure reinforces the idea that the two categories of disturbances can coexist (as also witnessed by the isosurfaces reported in Figure 28b, which have structure intermediate with respect to the disturbances visible in Figure 18c and Figure 23).

Figures 29 and 30, refer to the evolution of the field when the Rayleigh number is further increased. *Both relate to the same value of the Rayleigh number ($Ra = 2x10^4$), the main difference being represented by the considered initial conditions*, namely, a quiescent thermally diffusive field for Figure 29 and the already developed velocity field (shown in Figure 28) for Figure 30. It can be seen that, while the flow in Figure 29 is essentially dominated by OLRs, this hydrothermal mode coexists with hydrodynamic disturbances in Figure 30. These findings are in line with the general idea that in a problem where coexisting branches of solutions are possible, the trajectories of the system in the space of phases can be attracted selectively to either of the solutions according to the considered initial state.

As a concluding remark, we wish to highlight that additional insights into the dynamics presented in the last part of this chapter may follow naturally from direct comparison of the frequency spectra with theoretical data available in the literature about the time scale limiting the inertial

range of turbulence from below, i.e., the so-called Kolmogorov time scale (η_t).

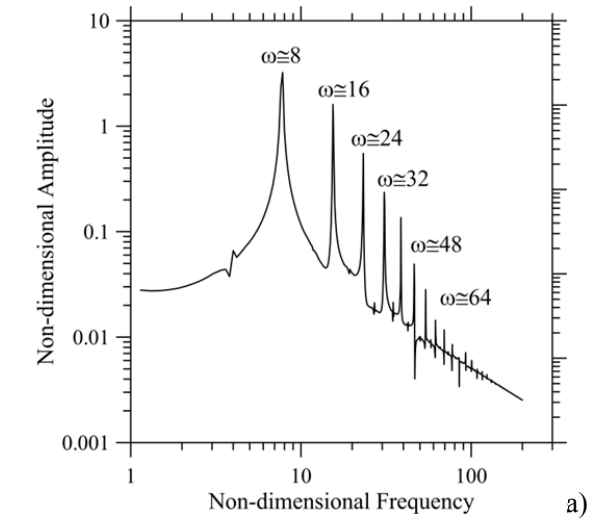

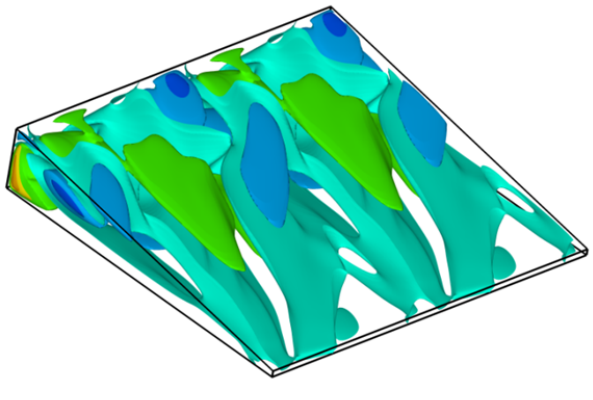

b)

Figure 29. Properties of the oscillatory state for Pr = 0.05, A_x = 10, A_z = 10, η = 0.1, periodic boundary conditions, initial conditions corresponding to a quiescent thermally diffusive state, Ra = 20000 (Gr = $4x10^5$): a) frequency spectrum, b) isosurfaces (snapshot) of the *w* component of velocity.

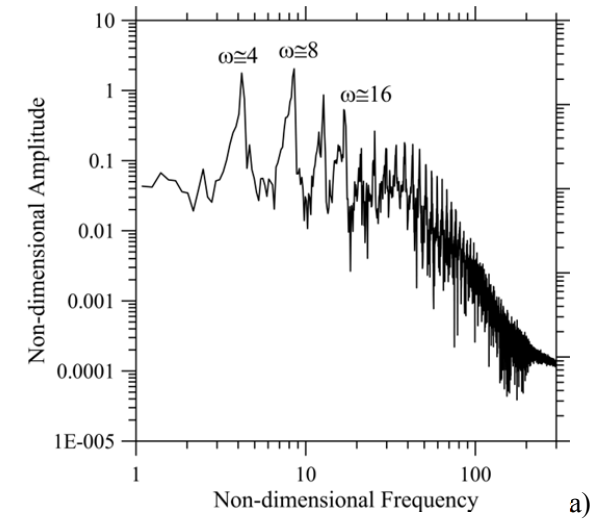

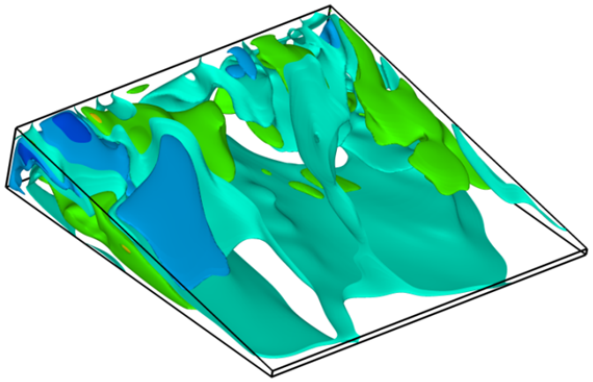

b)

Figure 30. Properties of the oscillatory state (mixed regime with hydrothermal and hydrodynamic modes) for Pr = 0.05, A_x = 10, A_z = 10, η = 0.1, periodic boundary conditions, Ra = 20000 (Gr = $4x10^5$), initial conditions corresponding to Figure 28b: a) frequency spectrum, b) isosurfaces (snapshot) of the *w* component of velocity.

Following Paolucci (1990) and Farhangnia et al. (1996), for a transversely heated cavity the Kolmogorov time and length scales can be evaluated, respectively, as:

$$\eta_t = 8\pi\left(\mathrm{Pr}\,Ra^3\right)^{-1/4} \tag{7a}$$

$$\eta_s = \pi\left(\frac{16\,\mathrm{Pr}}{Ra}\right)^{3/8} \tag{7b}$$

The good agreement between the right end of the intervals (shown in the preceding figures) where the Kolmogorov law is satisfied (for the case of 3D hydrodynamic disturbances) and the values provided by eq. (7a) led Lappa and Ferialdi (2018b) to the conclusion that these disturbances are the perturbations contributing more significantly to the transformative process leading these systems from low-dimensional chaos to fully developed turbulence.

CONCLUSION

The onset of typical instabilities in liquid metals undergoing buoyancy convection in differentially heated systems has been considered for different conditions and varying degrees of approximation. Starting from a review of results for infinite layers with horizontal or non-horizontal orientation produced in the past under the assumption of parallel flow and through the application of linear-stability-analysis techniques, we have considered configurations with progressively increasing complexity. These problems (relevant examples being represented by two-dimensional or three-dimensional cavities delimited by horizontal or non-horizontal solid walls) typically need to be addressed in the framework of advanced methods for the numerical solution of the overarching equations in their complete, time-dependent and non-linear form.

Initially, we have considered the typical behavior of these systems under the constraint of two-dimensional flow for which the emerging disturbances are expected to be purely hydrodynamic in nature (given the 3D nature of other perturbations such as the hydrothermal modes).

For the enclosures with converging or diverging walls and no net tilt, we have shown that three distinct regions of spatio-temporal behavior are

possible in the considered range of compression/expansion ratios. The central one ($\eta \cong 1$) is the region of "standard" hydrodynamic modes emergence, that is the area of the space of parameters (η, Ra) where the Hadley flow is affected by the typical 'pulsating' disturbances (P) already observed in past studies for the case of perfectly rectangular cavities. The two external regions ($\eta < 1$ and $\eta > 1$), however, correspond to a different type of hydrodynamic disturbances, which spread continuously along the horizontal direction resembling 'travelling waves'. Though, for relatively small values of Ra, these two types of disturbances manifest separately, they are not truly progressive, nor are they reciprocally exclusive. These modes witness the existence of 'multiple' states of convection. In some cases (essentially in the high-Ra part of the space of parameters), disturbances relating to different branches can coexist leading to a flow in which a low-frequency (traveling) perturbation is modulated locally by a high-frequency (pulsating) disturbance.

When fully 3D configurations are considered, the third dimension enables the onset and growth of disturbances of hydrothermal origin (for which the possibility to propagate in the spanwise direction is an essential prerequisite). Even more interestingly, the presence of the third dimension has also a remarkable effect on the properties of the hydrodynamic modes, which can appear as 3D disturbances since the beginning.

Though hydrothermal waves seem to be more frequent as the Prandtl number is increased and they apparently rule out the development of hydrodynamic disturbances (for relatively small values of the Rayleigh number), however, hydrodynamic disturbances overwhelmingly re-enter the dynamics as soon as the momentum and energy balance equations are uncoupled or the Grashof number is sufficiently increased. Both modes can exist as multiple solutions and manifest separately or in combined form as revealed by a careful analysis of the frequency spectra.

We have also shown how, according to whether the emerging chaos displays a low-dimensional or high-dimensional nature, a relevant characterization of these systems can be based on the evaluation of the 'fractal' (correlation) dimension or the typical laws of the so-called Kolmogorov 'inertial range' of turbulence, respectively.

Future work shall be devoted to analyses fluid flow in 2D and 3D geometries with converging or diverging walls considering a net tilt with respect to the horizontal direction for which convective modes of Rayleigh nature, not possible for the conditions considered in the present chapter, can enter the dynamics and make the overall scenario even more complex.

REFERENCES

Afrid M. and Zebib A., (1990), "Oscillatory three-dimensional convection in rectangular cavities and enclosures", *Phys. Fluids*, 2(8): 1318-1327.

Balatoni J. and Renyi A., (1956), "On the notion of entropy", *Publ. Math. Inst. Hung. Acad. Sci.* 1, 9 (in Hungarian) [translation: Selected papers of A. Renyi, Vol. 1 (Budapest Academy, 1976) p. 558].

Braunsfurth M.G. and Mullin T., (1996), "An experimental study of oscillatory convection in liquid gallium", *J. Fluid Mech*., 327: 199-219.

Chorin A.J., (1968), "Numerical solutions of the Navier-Stokes equations", *Math. Comput*., 22: 745-762.

Crespo del Arco E., Pulicani P.P. and Randriamampianina A., (1989), "Complex multiple solutions and hysteresis cycles near the onset of oscillatory convection in a Pr = 0 liquid submitted to a horizontal temperature gradient", *C. R. Acad. Sci. Paris* 309, II: 1869-1876.

De A.K., Eswaran V., Mishra P.K., (2017), "Scalings of heat transport and energy spectra of turbulent Rayleigh-Bénard convection in a large-aspect-ratio box", *Int. J. Heat Fluid Flow*, 67: 111–124.

Delgado-Buscalioni R., (2001), "Convection patterns in end-heated inclined enclosures", *Phys. Rev. E* 64, 016303 17 pages.

Delgado-Buscalioni R., Crespo del Arco E. And Bontoux P., (2001), "Flow transitions of a low-Prandtl-number fluid in an inclined 3D cavity", *Eur. J. Mech. B/Fluids*, 329: 1-17.

Drazin P. and Howard L.N., (1966), "Hydrodynamic stability of parallel flow of inviscid fluid", *Adv. Appl. Mech.*, 9: 1-89.

Dupret F. and Van der Bogaert N., (1994), "Modelling Bridgman and Czochralski growth", in *Handbook of Crystal Growth* (ed. D.T.J. Hurle) 2: 877-1010. North-Holland, Amsterdam (1994).

Farhangnia M., Biringen S, Peltier L.J., (1996), "Numerical Simulation of Two-dimensional Buoyancy-driven Turbulence in a Tall Rectangular Cavity", *Int. J. Numer. Meth. Fluids*, 23(12): 1311 - 1326.

Gelfgat A.Yu., Bar-Yoseph P.Z. and Yarin A.L., (1999), "Stability of Multiple Steady States of Convection in Laterally Heated Cavities", *J. Fluid Mech.*, 388: 315-334.

Gershuni G.Z., Laure P., Myznikov V.M., Roux B., Zhukhovitsky E.M., (1992), "On the stability of plane-parallel advective flows in long horizontal layers", *Microgravity Q.*, 2(3): 141-151.

Gill A.E., (1974), "A theory of thermal oscillations in liquid metals", *J. Fluid Mech.* 64 (3): 577-588.

Grassberger P. and Procaccia I., (1983a), "Characterization of Strange Attractors", *Phys. Rev. Lett*., 50: 346-349.

Grassberger P. and Procaccia I., (1983b), "Measuring the strangeness of strange attractors", *Physica D*, 9: 189-208.

Grassberger P., (1983), "Generalized dimensions of strange attractors", *Physics Letters A*, 97(6, 5): 227-230.

Gresho P.M., (1991), "Incompressible fluid dynamics: some fundamental formulation issues", *Ann. Rev Fluid Mech*., 23: 413-453.

Gresho P.M., Sani R.T., (1987), "On pressure boundary conditions for the incompressible Navier-Stokes equations", *Int. J. Numer. Meth. Fluids*, 7: 1111-1145.

Hadley G., (1735), "Concerning the cause of the general trade winds", *Phil. Trans. Roy. Soc. Lond.*, 29, 58-62.

Harlow F.H. and Welch J.E. (1965), "Numerical calculation of time-dependent viscous incompressible flow with free surface", *Phys. Fluids*, 8: 2182-2189.

Hart J.E., (1972), "Stability of thin non-rotating Hadley circulations", *J. Atmos. Sci*., 29: 687-697.

Hart J.E., (1983), "A note on the stability of low-Prandtl-number Hadley circulations", *J. Fluid Mech*., 132: 271-281.

Hung M.C. and Andereck C.D., (1988), "Transitions in convection driven by a horizontal temperature gradient", *Physics Letters A* 132(5): 253-258.

Kengne J., Nguomkam Negou A., Tchiotsop D., Kamdoum Tamba V., Kom G.H., (2018), "On the Dynamics of Chaotic Systems with Multiple Attractors: A Case Study", In: Kyamakya K., Mathis W., Stoop R., Chedjou J., Li Z. (eds) Recent Advances in Nonlinear Dynamics and Synchronization. *Studies in Systems, Decision and Control, vol* 109. Springer, Cham.

Kolmogorov, A.N. (1941a) "The local structure of turbulence in incompressible viscous fluids at very large Reynolds numbers", *Dokl. Akad. Nauk. SSSR* 30: 299-303. Reprinted in *Proc. R. Soc. London* A 434: 9-13 (1991).

Kolmogorov A.N., (1941b), "On the degeneration of isotropic turbulence in an incompressible viscous fluids", *Dokl. Akad. Nauk. SSSR* 31: 538-541.

Kolmogorov A.N., (1941c), "Dissipation of energy in isotropic turbulence", *Dokl. Akad. Nauk. SSSR*, 32: 19-21.

Kolmogorov A.N., (1942), "Equations of turbulent motion in an incompressible fluid", *Izv. Akad. Nauk. SSSR ser. Fiz*. 6: 56-58.

Kuo H.P. and Korpela S.A., (1988), "Stability and finite amplitude natural convection in a shallow cavity with insulated top and bottom and heated from the side", *Phys. Fluids*, 31: 33–42.

Ladyzhenskaya O.A., (1969), The Mathematical Theory of Viscous Incompressible Flow, Gordon and Breach, 2nd Edition, New York - London, 1969.

Lappa M., (1997), "Strategies for parallelizing the three-dimensional Navier-Stokes equations on the Cray T3E", in *Science and Supercomputing at CINECA*, Vol. 11, pp. 326-340.

Lappa M., (2002), "Well-posed problems for the Navier-Stokes equations in the microgravity environment", *Microgravity & Space Station Utilization* (ISSN: 0958-5036), 3(4): 51-62.

Lappa M., (2009), Thermal Convection: Patterns, Evolution and Stability, John Wiley & Sons, Ltd (2009, Chichester, England).

Lappa M., (2019), "*Convective effects and traveling waves in transparent oxide materials processed with the floating zone technique*", this book.

Lappa M. and Ferialdi H., (2018a), Multiple solutions, Oscillons and Strange Attractors in ThermoViscoElastic Marangoni Convection, *Phys. Fluids*, 30(10), 104104 (19 pages).

Lappa M. and Ferialdi H., (2018b), "Gravitational Thermal Flows of Liquid Metals in 3D Variable Cross-section Containers: Transition from low-dimensional to high-dimensional chaos", *Chaos*, 28, 093114 (21 pages).

Lappa M. and Ferialdi H., (2017), "On the Oscillatory Hydrodynamic Instability of Gravitational Thermal Flows of Liquid Metals in Variable Cross-section Containers", *Phys. Fluids*, 29(6), 064106 (19 pages).

Laure P. and Roux B., (1989), "Linear and non linear study of the Hadley circulation in the case of infinite cavity", *J. Cryst. Growth* 97(1): 226-234.

Lin C.-C., (1944), "On the stability of two-dimensional parallel flows", *Proc. NAS*, 30(10): 316-324.

Monberg E., "Bridgman and related growth techniques". In *Handbook of Crystal Growth* (ed. D.T.J. Hurle), 2: 53-97. North-Holland, Amsterdam (1994).

Moukalled F., Mangani L. and Darwish M., (2016), *The Finite Volume Method in Computational Fluid Dynamics - An Advanced Introduction with OpenFOAM and Matlab,* Springer International Publishing, 2016, New York).

Okada K. and Ozoe H., (1993b), "The Effect of Aspect ratio on the critical Grashof number for Oscillatory Natural Convection of Zero Prandtl Number Fluid: Numerical Approach", *J. Cryst. Growth*, 126: 330-334.

Okada K., and Ozoe H., (1993a), "Various computational conditions of oscillatory natural convection of zero Prandtl number fluid in an open boat heated and cooled from opposing vertical walls", *Numerical Heat Transfer*, Part A Applications, 23(2): 171-187.

Paolucci S., (1990), "Direct numerical simulation of two-dimensional turbulent natural convection in an enclosed cavity", *J. Fluid Mech*., 215: 229-262.

Pratte J.M. and Hart J.E., (1990), "Endwall driven, low Prandtl number convection in a shallow rectangular cavity", *J. Cryst. Growth*, 102: 54-68.

Pulicani J.P., Del Arco E.C., Randriamampianina A., Bontoux P., and Peyret R., (1990), "Spectral simulations of oscillatory convection at low Prandtl number", *Int. J. Numer. Meth. Fluids*: 10(5), 481-517.

Rosenbluth M.N. and Simon A., (1964), "Necessary and sufficient conditions for the stability of plane parallel inviscid flow", *Phys. Fluids*, 7(4): 557-558.

Squire H.B., (1933), "On the stability of three-dimensional disturbances of viscous flow between parallel walls", *Proc. R. Soc. London, Ser. A*, 142: 621-628.

Temam R., (1968), "Une méthode d'approximation de la solution des équations de Navier-Stokes", *Bull. Soc. Math. France*, 98: 115-152.

Theiler J., (1986), "Spurious dimension from correlation algorithms applied to limited time-series data", *Physical Review A*, 34(3): 2427-2432.

Tollmien W., (1936), "General instability criterion of laminar velocity distributions", *Tech. Memor. Nat. Adv. Comm. Aero.*, Wash. No. 792 (1936).

Wakitani S., (2001), "Numerical study of three-dimensional oscillatory natural convection at low Prandtl number in rectangular enclosures", *J. Heat Transfer*, 123: 77-83.

RR